JOURNAL OF THERMOPHYSICS AND HEAT TRANSFER
Vol. 24, No. 3, July–September 2010

Acceleration Effects on the Cooling Performance of a Partially Confined FC-72 Spray

Travis E. Michalak* and Kirk L. Yerkes†
U.S. Air Force Research Laboratory, Wright-Patterson Air Force Base, Ohio 45433
Scott K. Thomas‡
Wright State University, Dayton, Ohio 45435
and
John B. McQuillen§
NASA John H. Glenn Research Center at Lewis Field, Cleveland, Ohio 44135

DOI: 10.2514/1.46547

This paper discusses the effects of a variable-gravity environment on the performance of a subcooled partially confined spray. An experiment consisting of a test chamber, associated flow loops, and instrumentation was fabricated and flown on the NASA Reduced-Gravity Testing Platform. This modified KC-135 aircraft followed a parabolic flight path to provide various acceleration levels. The spray chamber contained a nozzle spraying onto an upward-facing thick-film resistor heater, which was mounted on an insulating glass pedestal. Thermocouples under the heater in the glass pedestal were used to determine the heater surface temperature. The glass pedestal was surrounded by an annular sump system, which was used to collect and remove the cooling fluid from the test chamber. The fluid used for this testing was FC-72, which is a nontoxic, nonflammable, and nonreactive refrigerant. Because of its dielectric nature, FC-72 was sprayed directly onto the thick-film heater. The parametric ranges of this experiment were as follows: heat flux to the spray was $21.1 \le q''_{sp} \le 69.0$ W/cm^2, acceleration field was $0.15 \le a \le 1.80$ g, coolant volumetric flow rate was $6.18 \le V \le 8.94$ ml/s, and coolant subcooling was $23.1 \le \Delta T_{sc} \le 31.7$ K. The heat fluxes tested were below the critical heat flux q''_{CHF}. The wall superheat $\Delta T_{sat} = T_s - T_{sat}$ was found to increase with heat input and acceleration and to decrease with subcooling and volumetric flow rate.

Nomenclature

A	=	heater area, m^2
a	=	acceleration normal to surface, g
b	=	radius of glass heater post assembly, m
C	=	percent dissolved air content by volume, $[V'_{air}/(V'_f + V'_{air})] \times 100$
D	=	diameter, m
E	=	voltage, V
f	=	heater conduction loss fraction, $1 - (q''_{sp}/q''_H)$
H	=	layer thickness, m
h	=	convective heat transfer coefficient, W/(m^2 − K)
k	=	thermal conductivity, W/(m − K)
m	=	mass flow rate, kg/s
Nu	=	Nusselt number, $h_{top}b/k_f$
P	=	pressure, N/m^2
q	=	power, W
q''	=	heat flux, W/cm^2
R	=	electrical resistance, Ω
T	=	temperature, K
V	=	volumetric flow rate, ml/s
V'	=	volume, m^3
v	=	droplet velocity, m/s
We	=	Weber number, $\rho v^2 D_d/\sigma$
ΔT	=	temperature difference, K
ΔT_{sat}	=	wall superheat, $T_s - T_{sat}$, K
ΔT_{sc}	=	fluid subcooling temperature, $T_{sat} - T_{noz}$, K
θ	=	nondimensional temperature, $(T - T_{\infty,wall})/(T_{sat} - T_{\infty,wall})$
ρ	=	density, kg/m^3
σ	=	surface tension, kg/s^2

Subscripts

air	=	air
ch	=	chamber
CHF	=	critical heat flux
cov	=	glass cover layer
d	=	droplet
f	=	freestream fluid
H	=	heater
htr	=	heater layer
int	=	heater/pedestal interface
l	=	liquid
lf	=	lower film
MHF	=	minimum heat flux
noz	=	nozzle inlet
P	=	precision
R	=	resistor
s	=	surface
sat	=	saturation
sc	=	subcooling
sp	=	spray
sub	=	ceramic substrate layer
top	=	surface of heater
uf	=	upper film

Presented as Paper 2007-198 at the 45th AIAA Aerospace Sciences Meeting and Exhibit, Reno, NV, 8–11 January 2007; received 9 November 2009; revision received 19 February 2010; accepted for publication 1 March 2010.

*Mechanical Engineer, Propulsion Directorate, Energy/Power/Thermal Division, Thermal and Electrochemical Branch, 1950 5th Street, Building 18. Member AIAA.

†Deputy for Science, Propulsion Directorate, Energy/Power/Thermal Division, 1950 5th Street, Building 18. Associate Fellow AIAA.

‡Associate Professor, Department of Mechanical and Materials Engineering, 3640 Colonel Glenn Highway. Associate Fellow AIAA.

§Aerospace Engineer, Microgravity Fluid Physics Branch.

v = vapor
∞,top = freestream fluid flowing over heater surface
∞,wall = freestream fluid flowing over pedestal wall

Introduction

THE thermal management of high-power, high-flux devices is becoming increasingly difficult. Even with advances in materials and efficiencies, these devices require the dissipation of ever increasing amounts of thermal energy. Many of these devices also have both low thermal mass and tight spatial and temporal isothermality requirements, sometimes less than ± 2 K. For devices being used for aerospace applications, the systems are additionally required to operate under various acceleration levels. As a result, robust thermal management approaches need to be developed. Spray cooling is a thermal management scheme that has the potential to be a solution to many of these challenges [1,2], including the cooling of electronic devices, which often require the removal of high heat fluxes at low surface superheats [3,4]. However, it is not yet clear what influence variable-gravity environments might have on the behavior of spray-cooling systems. Kim [5] stated that gravity can have an effect on the performance of multiphase thermal management systems, but did not discuss spray cooling. There have been several specialized applications of spray cooling for aerospace applications. For instance, the Space Shuttle Orbiter uses spray evaporators with water and ammonia as the working fluids [6]. This spray system operates in an open-loop configuration and uses brief pulses of the working fluid, which is nearly completely evaporated [7]. However, for spray cooling to be a viable thermal management technique for widespread aerospace applications, a greater understanding of the behavior of this scheme under variable-gravity conditions needs to be developed, especially using a closed-loop, recirculating system.

In spray cooling, a working fluid is forced through an orifice and atomized into small drops. These drops then impinge on the surface to be cooled and remove large amounts of heat through a combination of single-phase convection and evaporation [2]. Sehmbey et al. [8] identified two types of spray cooling: Pressure atomization and gas-assisted atomization. In pressure-atomized nozzles, the working fluid is atomized through the pressure drop across the nozzle, whereas with gas-assisted atomization, a high-velocity gas (or vapor) is used to break the working fluid up into droplets. Spray cooling can have many advantages over standard heat spreader/forced air cooling for electronics applications, including improved performance and reduced size and noise [9]. Spray cooling can have advantages over other forms of two-phase cooling as well. Sehmbey et al. [8] suggested that spray-cooling heat transfer and q''_{CHF}, the maximum heat transfer obtainable through nucleate boiling, can be 10 times higher than values obtained using pool boiling.

Kim [2] discussed heat transfer mechanisms involved in spray cooling, as well as some of the factors that influence the performance of spray cooling, such as surface condition and size, spray pattern and droplet characteristics, working-fluid properties, the presence of noncondensable gases, spray inclination, and gravity. Silk et al. [7] also gave an overview of spray-cooling research and details on planned future work in variable-gravity spray cooling, especially for microgravity applications.

Some of the early efforts into spray cooling found that the characteristics of the spray can have a significant effect on heat transfer performance. The droplets of the spray have to be large enough and move fast enough to reach the surface through any escaping vapor, yet be small enough and move slowly enough that they do not simply bounce off the surface. The amount of excess fluid used should be minimized to keep the liquid film on the surface as thin as possible. This recommendation was due to the fact that the two-phase heat transfer that takes place in spray cooling is optimal when thin-film evaporation occurs, as opposed to the nucleate boiling that takes place in pool boiling [10,11]. However, it should be noted that Estes and Mudawar [12] found that for sprays with relatively high volumetric fluxes, the boiling curve does not necessarily look like the traditional boiling curve as there was very little change in slope between the single-phase and nucleate boiling regimes. This was attributed to a suppression of nucleate boiling and the presence of excess fluid leading to low evaporation efficiency.

Pautsch and Shedd [13] reported that systems that did not use fluid as effectively and relied more on single-phase cooling, tended to be able to reach higher values of q''_{CHF}. In fact, based on models that were developed from experimental data, it was reported by Shedd and Pautsch [14] that the heat removal can be primarily attributed to single-phase mechanisms. In contrast, Lin et al. [15] reported that the spray-cooling performance could be attributed, in a large part, to nucleate boiling. This conclusion was reached through single-nozzle spray-cooling experiments performed with water, methanol, or a combination of water and methanol.

Pais et al. [11] examined the impact of subcooling and flow rate on the performance of spray cooling using air-atomizing nozzles and water. The results showed that a fluid with a larger subcooling, ΔT_{sc}, tends to remove more heat from the surface before the onset of nucleate boiling, while a fluid with a smaller ΔT_{sc} may remove more heat in the region near q''_{CHF}, depending on the spray characteristics. The results also indicated that higher liquid flow rates removed more heat in the region before the onset of nucleate boiling and in the q''_{CHF} region.

Puterbaugh [16] and Puterbaugh et al. [17] used a test rig similar to that described in Baysinger et al. [18] and Yerkes et al. [19] to test the effect of air dissolved into the working fluid on spray-cooling performance. Dissolved air content was measured using a mercury Aire-ometer and was varied between $5\% \leq C \leq 18\%$. It was reported that there was little change in spray-cooling heat transfer performance with varying air content for the range of chamber pressures, flow rates, and subcooling levels tested.

Um et al. [20] investigated the effect of heater surface orientation on q''_{CHF} for spray cooling. The various surface orientations are described in Fig. 1. Two different air-atomizing nozzles were used to spray water at different liquid flow rates onto a heated surface which could be oriented horizontally facing upward, vertically, or horizontally facing downward. One nozzle had a uniform spray pattern, while the other had a nonuniform spray pattern, with the flow more heavily concentrated in the center of the pattern. The orientation of the surface showed little effect on q''_{CHF} for the uniform-spray nozzle. There was also little difference noted between the upward- and downward-facing horizontal orientations for the nonuniform spray. However, q''_{CHF} was found to be higher for the vertically oriented surface than for the horizontally oriented surface when using the nonuniform spray, and the percentage change in q''_{CHF} was less at higher liquid flow rates.

Lin and Ponnappan [21] reported on the spray-cooling performance for an eight-nozzle array spraying on a surface with

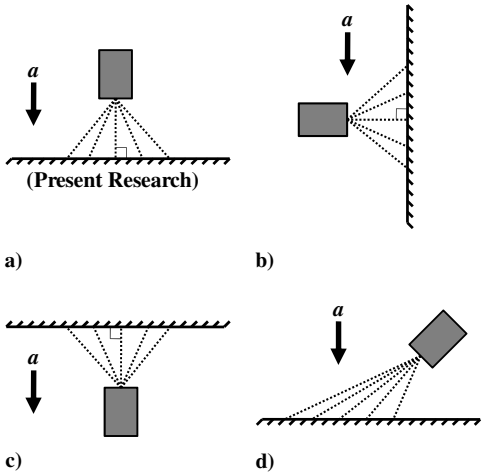

Fig. 1 Orientation schematics: a) upward-facing horizontal, as in the present research; b) vertical; c) downward-facing horizontal; and d) inclined spray.

an area of 2.0 cm^2, using FC-87, FC-72, methanol, and water as the working fluids, at low levels of subcooling (FC-87: $\Delta T_{sc} < 0.6°C$, FC-72: $\Delta T_{sc} < 3.5°C$, methanol: $2.7 < \Delta T_{sc} < 13.7°C$, and water: $3.0 < \Delta T_{sc} < 14.1°C$). It was found that ΔT_{sat} increased with increasing heat flux. Both the heat flux that could be removed at a given ΔT_{sat} and q''_{CHF} increased as volumetric fluxes increased. For the fluorocarbon fluids FC-72 and FC-87, q''_{CHF} was up to 90 W/cm^2. Methanol produced q''_{CHF} of 490 W/cm^2, and for water, q''_{CHF} exceeded the maximum achievable heat flux for this system, which was 500 W/cm^2. The heat transfer coefficient followed a similar trend; water yielded the highest, followed by methanol, and then the fluorocarbon fluids.

Lin et al. [22] reported on the effects of surface orientation on the performance of spray cooling a large area (19.3 cm^2) using a 48-nozzle array. It was reported that both the cooling performance and q''_{CHF} were slightly enhanced for the case of a downward-facing horizontal surface, when compared to a vertical surface. The performance of this setup was also compared to that obtained using the small (2.0 cm^2) area heater from Lin and Ponnappan [21]. The cooling performance of the small-area heater (in an upward-facing horizontal orientation) was more than 30% better than for the vertically oriented large-area heater.

Lin and Ponnappan [23] also reported on the behavior of large-area spray cooling at different surface orientations. During this effort, an ejector was used to improve the stability of the flow rate by employing the motive flow produced by a gear pump to produce suction at the exit of the condenser, which assisted in ensuring that no vapor was allowed to enter the inlet of the gear pump. The downward-facing horizontal heater had a 5% higher q''_{CHF} than the vertically oriented heater, and the vertically oriented heater had a 6% higher q''_{CHF} than the upward-facing horizontal heater.

Rybicki and Mudawar [24] reported on the effects of various parameters including orientation on spray-cooling performance. Several correlations were developed in previous works [12,25,26] using upward-facing horizontal surfaces. In this effort, a downward-facing horizontal surface was used with PF-5052 as the working fluid. These new data were found to be described by the same correlations for multiple regions of the boiling curve. Since the same correlations could be applied to all of the data, it was concluded that the nozzle/surface orientation had little effect on performance, as long as large amounts of liquid were not allowed to build up on the surface in an upward-facing horizontal surface orientation.

Kato et al. [27] examined the effects of both heater orientation (under terrestrial conditions) and acceleration (provided by an aircraft following a parabolic trajectory) on the cooling performance of sprays. Two working fluids were used with the same pressure-atomized nozzle. For water, the spray was found to be uniform, and for CFC-113, the spray was found to be nonuniform. For these experiments, a copper block with a nickel-plated surface was heated to a high temperature and then cooled down over a period of time consisting of 10 parabolas for the flight tests. The flow rate was generated with a pressurized piston/cylinder as opposed to a recirculating closed loop. During the terrestrial heater orientation tests with water, q''_{CHF} was found to be slightly higher for a vertical surface than for an upward-facing horizontal surface. Also, in the transition boiling region (above q''_{CHF}), for a given heat flux, the wall superheat ΔT_{sat} was higher for the vertical surface than for the upward-facing horizontal surface. During parabolic flight testing with CFC-113, q''_{CHF} was found to decrease in reduced gravity, and for a given heat flux, ΔT_{sat} was lower in reduced gravity, especially in the transition region above q''_{CHF}. With water, q''_{CHF} was higher in reduced gravity than in terrestrial or elevated gravity, but for a given heat flux, ΔT_{sat} was again found to be lower in reduced gravity, though this gravity dependence was more pronounced in the region below q''_{CHF} for water. Gravity dependence was not reported for a higher spray volume flux of water.

Sone et al. [28] reported on a continuation of the work by Kato et al. [27], again using a pressurized piston/cylinder to generate the flow rate. Water and FC-72 were examined, using several different nozzles. Using a transparent indium tin oxide (ITO) heater, the effect of orientation under terrestrial gravity conditions was again studied. For water, heaters oriented both vertically and downward-facing horizontally showed decreased heat transfer when compared to an upward-facing horizontally oriented heater, while FC-72 sprays did not show an appreciable dependence on heater orientation. Also using this ITO heater, the heat transfer performance of a water spray was shown to be degraded slightly with a reduction in gravity in the region below q''_{CHF}. With this transparent heater, differences were noted between water and FC-72 in the behavior of the impacting droplets, the liquid film, and the heater surface. The water liquid film was reported to be stagnant, and the thickness seemed to be dependent on gravity or heater orientation. The FC-72 film was more prone to being swept away by impacting droplets, possibly due to significant differences in thermophysical properties such as viscosity and surface tension between water and FC-72.

The results for tests with a copper block heater with a Cr-plated surface were also presented by Sone et al. [28]. The heater was heated to a high temperature and then cooled during the parabolas. For water at low spray volume fluxes, in the region below q''_{CHF} and in the film boiling region above the minimum heat flux point, q''_{MHF}, the heat transfer decreased with a decrease in gravity. For the smallest tested spray volume flux conditions with water in the high ΔT_{sat} region, heat transfer was degraded in reduced gravity. For water with high spray volume fluxes, reducing gravity tended to result in a reduced q''_{CHF}. For FC-72, a spatial variation in gravity dependence was reported. Near the center of the heater, decreasing gravity led to increased q''_{CHF} and enhanced heat transfer in the region below q''_{CHF}, while thermocouples near the edge of the heater showed an opposite effect.

Further experiments were carried out by Yoshida et al. [29], in which a copper block heater with a Cr-plated surface and a transparent ITO heater were employed, along with three different nozzles, with water and FC-72. The spray volume fluxes used were small enough that the heater surface was not completely covered by liquid, but remained in a dropwise evaporation regime and were again generated using a pressurized piston/cylinder. The copper block heater was used to perform transient cooling tests by heating it up to a high temperature at the beginning of a flight and then cooling it down over a period of 10 parabolas. The ITO heater was used to provide steady-state heat transfer results by supplying a set heater power and spraying the surface. Gravity was not observed to have a strong effect on the spray-cooling performance in the nucleate boiling regime for either fluid. For water in terrestrial conditions, a downward-facing horizontal heater produced a higher heat flux than an upward-facing horizontal heater. For low spray volume fluxes, q''_{CHF} was not affected by gravity or heater orientation, but q''_{CHF} and heat transfer in the transition boiling region (between q''_{CHF} and the film boiling region) was affected by gravity and heater orientation for higher spray volume fluxes. The strongest effect of gravity and orientation was observed in the q''_{MHF} region and the film boiling region for low Weber numbers. With a downward-facing heater in both terrestrial and reduced gravity, the heat flux was reduced for these low-Weber-number tests.

Golliher et al. [6] used a drop tower located at NASA John H. Glenn Research Center at Lewis Field, capable of producing 2.2 s of microgravity, to study the behavior of a spray striking a flat surface. The experiment was performed with an air-atomized nozzle spraying water onto an aluminum surface, with and without heat input to the surface and without the use of a recirculating closed loop. Upon striking the surface, the spray was observed to form multiple separated segments of coalesced liquid, arranged in a repeatable pattern. This has significant implications in the management and removal of any working fluid that is not evaporated during the cooling process. This paper concentrated on the physical behavior of the spray and did not include information on the cooling performance of the spray system.

Roisman et al. [30] reported on the behavior and splashing of droplets striking a convex surface in microgravity. Three different splash scenarios were identified, and a stability analysis and a nondimensional analysis were performed to attempt to predict the behavior of these phenomena. Gambaryan-Roisman et al. [31] reported on the behavior of the film produced by the impact of a water

spray on a heated convex surface, and the cooling performance of this spray-cooling scheme, in normal and reduced-gravity conditions. The flow rates were generated using a pressurized membrane tank, as opposed to a recirculating closed loop. It was found that the film thickness and the shape of the liquid/gas interface were affected by the parameters of the spray. The volumetric flow rate of the water had an impact on the film thickness and the spray-cooling performance. The gravity level was found to have an effect on the spray-cooling performance, especially for higher water flow rates, and a decrease in spray-cooling performance was noted in microgravity.

Rowden et al. [32] described the development of a closed-loop spray system that was designed to mimic an electronics package and to act as a precursor to future flight test benches for possible testing in microgravity environments. Also presented were the results of modeling efforts examining single bubble growth in a thin liquid film and the behavior of a single droplet of liquid striking a thin film of liquid near a bubble. The model accounted for the effects of gravity, and the variation in the average $Nu = q''[\sigma/a(\rho_l - \rho_v)]^{1/2}/(\Delta T_{\text{sat}} k_l)$ over time was found to be very similar between models using terrestrial gravity and microgravity. From these models, Rowden et al. [32] predicted that experimental data taken in terrestrial gravity may be applicable to microgravity environments. However, Selvam et al. [33] noted that computer modeling of spray cooling is a very complex task and gave an overview of some of the modeling efforts that have taken place, along with results of the modeling of a vapor bubble growing on a surface. There have been several other modeling efforts described in literature that concentrated mainly on the behavior of individual droplets or vapor bubbles [34–38]. Cole et al. [39] also presented results of spray-cooling modeling and included both a microscale model to predict behavior of an individual droplet and a macroscale model to predict behavior of a large number of droplets in a spray.

Some of the first research using a closed-loop recirculating test setup in a variable-gravity environment was accomplished by Baysinger et al. [18], who presented the design and preliminary testing of a variable-gravity spray-cooling experiment. The primary purpose of this study was to investigate heat transfer and fluid management issues for a continuous-flow, closed-loop spray-cooling system subjected to a variable-gravity environment. Tests were conducted using ITO heaters onboard the NASA KC-135 Reduced-Gravity Research Aircraft, which provided the variable-gravity environment by following a parabolic flight trajectory. This preliminary testing provided much information on the fluid management aspects of variable-gravity testing [40].

Building on the work by Baysinger et al. [18], Yerkes et al. [19] performed experiments using the same apparatus on the NASA KC-135 with ITO heaters, but with higher heat loads than the previous experiments. For these tests, the parameters ranges reported were Heat flux, $10.1 \leq q''_{\text{sp}} \leq 39.4$ W/cm^2; volumetric flow rate, $5.26 \leq V \leq 10.5$ ml/s; and acceleration, $0.01 \leq a \leq 1.8$ g. During this testing, the temperature difference between the surface and the fluid was found to decrease with decreasing acceleration. However, this testing was primarily in the single-phase region. It was determined that the ITO heaters were prone to failure at high heat loads, even with adequate cooling, due to high current densities in the thin resistive film.

Elston [41] and Elston et al. [42–44], reported the behavior of a 16-nozzle spray array in variable-gravity conditions. The test rig described in Baysinger et al. [18] and Yerkes et al. [19] was modified to test a custom-fabricated 16-nozzle spray array, cooling a thick-film resistor (TFR) heater with an area of 25.4×25.4 mm^2, for the following parametric ranges: Mass flow rate, $0.0131 \leq m \leq 0.0213$ kg/s; subcooling, $1.6 \leq \Delta T_{\text{sc}} \leq 18.4$°C; heat flux, $2.9 \leq q''_{\text{sp}} \leq 25$ W/cm^2; dissolved air content, $10.1 \leq C \leq 16.8$%; and acceleration, $0.02 \leq a \leq 2.02$ g. It was found that microgravity conditions provided enhanced spray-cooling performance, indicated by a lower ΔT_{sat} for a given heat input, except at high mass flow rates, where the microgravity performance was closer to that of the terrestrial- or elevated-gravity conditions. Higher levels of subcooling tended to provide enhanced performance, and the air content did not significantly affect performance for the range of parameters tested. The qualitative performance of an improved liquid–vapor separator was also discussed.

Shedd [45] described a linear spray array designed to impact a heated surface at an angle to avoid fluid management issues and loss of heat transfer performance due to interactions between multiple spray cones associated with cooling using arrays of spray nozzles. Conrad et al. [46] reported on the use of this type of array in variable-gravity testing. This research concluded that coolant flow rate had the largest effect on spray-cooling performance. It was found that reduced-gravity provided slightly increased heat transfer coefficients when compared to elevated-gravity conditions. The linear spray array used for this testing suffered a rupture in one of the seals, which redirected some of the flow away from the heater surface, so the flow rate of fluid on the heater surface may have been somewhat lower that what was reported.

Hunnel et al. [47] reported on initial experiments using a test rig to examine the effect of body forces generated using electrical fields on spray cooling. A single nozzle spraying on heated surfaces consisting of both an ITO and a TFR heater mounted on glass pedestals was used to measure the heat transfer performance of spray cooling in several different orientations. The heater pedestal was surrounded by an annular sump system, and several different containment cap configurations were examined. The ITO heater was found to have slightly higher heat transfer performance than the TFR heater, and for the highest flow rate tested, the horizontal spray orientation had slightly better performance than the vertically oriented spray. For lower flow rates, there was not a significant difference reported between the horizontal and vertical orientations. Because of this, the authors determined that a horizontal spray may not be adequate for predicting the behavior of sprays in a reduced-gravity environment.

Glaspell [48] continued the work by Hunnel et al. [47] by examining the effect of an electric Kelvin force on the performance of spray cooling. The objective was to provide more control over the fluid management and bubble behavior. Various electrodes, heaters, and fluids were tested, and the temperature difference between the surface and the fluid was reduced by a maximum of 1.91°C by applying an electrode voltage of 23 kV. This corresponded to an increase in the heat transfer coefficient of 5.2%. Kreitzer [49] and Kreitzer et al. [50] also looked at electrical fields to try to enhance spray-cooling performance. Instead of examining the electric Kelvin force, this research concentrated on the effect of the Coulomb force through inductively imparting an electrical charge on the droplets before impingement. A heat transfer improvement of up to 17% was reported, along with results for several heaters, fluids, electrodes, and nozzle types. However, variations of 5 to 14% were reported in the results obtained using different nozzles, though it was speculated that this variation may have been due to differences in nozzle alignment.

Coulomb force effects on spray-cooling performance were reported by Kuhlman et al. [51]. From flow visualization studies, it was determined that the characteristic time scales governing the effects of various parameters were not as short as the average time between droplet impacts. Further work to enhance spray heat transfer performance, potentially for variable-gravity environments, was discussed by Kreitzer et al. [52]. In this effort, a voltage was applied to the spray nozzle itself to charge the droplets. It was reported that the spray pattern changed, but the heat transfer performance remained the same. Kreitzer and Kuhlman [53] also reported on the behavior of sprays when a voltage was applied to the nozzle and presented the results of visualization.

As can be seen in the previous discussion, there is a wide range of results presented in the archival literature for various parameters that affect spray-cooling performance. Oftentimes, there were conflicting results presented, sometimes by the same researchers in the same publication. Tables 1–4 give a summary of the major findings of some of the studies that have examined the effects of orientation and variable-gravity environments on spray-cooling behavior. There remains much about the physical phenomena involved in spray cooling that is not well understood.

Table 1 Summary of acceleration results from [20,27,28]

a, g	Orientation	Nozzle configuration	Heater size	Heater type	Working fluid	Flow rate/ volume flux	T_{sat}, °C	ΔT_{sc}, K	q'', W/cm^2	$T_s - T_{sat}$, K	q''_{CHF}, W/cm^2	Orientation/ acceleration trends	Comments
						Kato et al. [27] (1995)							
1.0	Figs. 1a and 1b	[a]	19 mm diam	[b]	Water	2.0×10^{-3} to 8.5×10^{-3} m^3/m^2-s	100	80–83	30–400	0–220	170–400	$q''_{CHF} \uparrow$ for Fig. 1b than for Fig. 1a; $\Delta T_{sat} \uparrow$ for Fig. 1b than for Fig. 1a	More effect on ΔT_{sat} in transition boiling region
0.01, 1.0	Fig. 1a	[c]	19 mm diam	[b]	CFC-113	2.93×10^{-3} m^3/m^2-s	48	35–37	20–80	0–80	70–80	$q''_{CHF} \downarrow$ for $a \downarrow$, $\Delta T_{sat} \downarrow$ for $a \downarrow$	More effect on ΔT_{sat} in transition boiling region
0.01, 1.0, 1.5	Fig. 1a	[a]	19 mm diam	[b]	Water	2.51×10^{-3} m^3/m^2-s	100	88–92	40–230	0–200	180–230	$q''_{CHF} \uparrow$ for $a \downarrow$, $\Delta T_{sat} \downarrow$ for $a \downarrow$	More effect on ΔT_{sat} in region below q''_{CHF}
0.01, 1.0, 1.5, 2.0	Fig. 1a	[a]	19 mm diam	[b]	Water	5.35×10^{-3} m^3/m^2-s	100	84–87	60–300	0–220	280–300	Little change in q''_{CHF} or ΔT_{sat} with change in a	——
						Um et al. [20] (1996)							
1.0	Figs. 1a and 1b	Single, air-atomized, unconfined, uniform liquid flux	8×8 mm^2	[d]	Water	0.02 to 0.04 l/ min	N/A	N/A	0–525	$20 \leq T_s \leq 160$°C	200–525	No effect on q''_{CHF} due to orientation	——
1.0	Figs. 1a–1c	Single, air-atomized, unconfined, nonuniform liquid flux	8×8 mm^2	[d]	Water	0.01 to 0.03 l/ min	N/A	N/A	0–1300	$20 \leq T_s \leq 200$°C	300–1300	q''_{CHF} same for Fig. 1a and 1c; $q''_{CHF} \uparrow$ for Fig. 1b	Higher liquid mass flux at center of spray cone
						Sone et al. [28] (1996)							
1.0	Figs. 1a–1c	[a]	18×18 mm^2	[e]	Water	1.51×10^{-4} m^3/m^2-s	100	76	10–44	0–52	No	$\Delta T_{sat} \downarrow$ for Fig. 1a than Fig. 1b or Fig. 1c	——
1.0	N/A	N/A	18×18 mm^2	[e]	FC-72	N/A	56	N/A	N/A	N/A	No	No effect of heater orientation reported	——
0.01, 2.0	Fig. 1a	[f]	50 mm diam	[g]	Water	1.57×10^{-3} m^3/m^2-s	100	58–75	30–135	0–300	125–135	$q''_{CHF} \downarrow$ for $a \downarrow$, $\Delta T_{sat} \downarrow$ for $a \downarrow$ in transition and film boiling	Some discrepancy between plots and text
0.01, 2.0	Fig. 1a	[a]	50 mm diam	[g]	Water	1.51×10^{-4} m^3/m^2-s	100	62–80	3–31	0–300	31	No effect on q''_{CHF}; $q'' \downarrow$ for $a \downarrow$ in high ΔT_{sat} film boiling region	——
0.01, 2.0	Fig. 1a	[a]	18×18 mm^2	[e]	Water	1.51×10^{-4} m^3/m^2-s	100	18	14–34	4–48	No	$\Delta T_{sat} \uparrow$ for $a \downarrow$	——
0.01, 2.0	Fig. 1a	[f]	50 mm diam	[g]	FC-72	1.34×10^{-3} m^3/m^2-s	56	29	6–46	12–78	40–46	$q''_{CHF} \uparrow$ for $a \downarrow$, $\Delta T_{sat} \uparrow$ for $a \downarrow$ in transition boiling, $q'' \uparrow$ for $a \downarrow$ in film boiling	Some discrepancy between plots and text; opposite trend near heater edge

[a]Single, unconfined, pressure-atomized, uniform. [b]Ni-plated, Cu-block, cartridge heaters. [c]Single, unconfined, pressure-atomized, hollow cone. [d]Cu-block, lamps. [e]Pyrex block, ITO heater. [f]Single, unconfined, pressure-atomized, high mass flux at center. [g]Cr-plated, Cu-block, cartridge heaters.

Table 2 Summary of acceleration results from [21,22,29]

a, g	Orientation	Nozzle configuration	Heater size	Heater type	Working fluid	Flow rate/ volume flux	T_{sat}, °C	ΔT_{sc}, K	q'', W/cm^2	$T_s - T_{sat}$, K	q''_{CHF}, W/cm^2	Orientation/ acceleration trends	Comments
						Yoshida et al. [29] (2001)							
1.0	Figs. 1a and 1c	[a]	18 × 18 mm^2	[b]	Water	1.35×10^{-4} to 4.3×10^{-4} m^3/m^2-s	100	68–79	5–55	0–80	No	$\Delta T_{sat}\downarrow$ for Fig. 1c than for Fig. 1a	[c]
1.0	Figs. 1a and 1c	[a]	50 mm diam	[d]	Water	1.97×10^{-4} m^3/m^2-s	100	74.9	1–47.5	0–290	47.5	No orientation effect on q''_{CHF} or transition boiling; $q''\downarrow$ for Fig. 1c than for Fig. 1a in film boiling	[c]
1.0	Figs. 1a and 1c	[a]	18 × 18 mm^2	[b]	FC-72	N/A	56	29–37	N/A	N/A	No	$\Delta T_{sat}\downarrow$ for Fig. 1c than for Fig. 1a	[c]
1.0	Figs. 1a and 1c	[a]	50 mm diam	[d]	FC-72	2.17×10^{-3} m^3/m^2-s	56	30.3	0–11.5	0–95	10–11.5	q''_{CHF} and $q''_{MHF}\downarrow$ for Fig. 1c than for Fig. 1a, $q''\downarrow$ for Fig. 1c than for Fig. 1a in transition and film boiling	[c]
0.01, 1.0,2.0	Fig. 1a	[a]	18 × 18 mm^2	[b]	Water	1.4×10^{-4} to 3.7×10^{-3} m^3/m^2-s	100	68–79	N/A	N/A	No	No effect of change in accel reported	[c]
0.01, 1.0,2.0	Fig. 1a	[a]	50 mm diam	[d]	Water	1.42×10^{-4} m^3/m^2-s	100	79.1	0.5–24	20–260	24	q'' and $q''_{MHF}\downarrow$ for $a\downarrow$ film boiling; no accel effect elsewhere in boiling curve	[c]
0.01,1.0, 2.0	Fig. 1a	[a]	50 mm diam	[d]	Water	3.7×10^{-3} m^3/m^2-s	100	79.1	30–260	10–210	250–260	$q''_{CHF}\uparrow$ for $a\downarrow$; $\Delta T_{sat}\uparrow$ for $a\downarrow$ in transition boiling; no accel effect in film boiling	[c]
0.01, 2.0	Fig. 1a	[a]	18 × 18 mm^2	[b]	FC-72	2.25×10^{-4} m^3/m^2-s	56	31.5	4.3–6.6	8–38	No	No effect of change in accel reported	[c]
0.01, 2.0	Fig. 1a	[a]	50 mm diam	[d]	FC-72	2.2×10^{-4} m^3/m^2-s	56	31–36.9	1–19.5	20–80	16–19.5	$q''\downarrow$ for $a\downarrow$ in film boiling for low Weber number; no effect of accel reported elsewhere	[c]
						Lin and Ponnappan [21] (2003)							
1.0	Fig. 1a	[e]	1.0 × 2.0 cm^2	[f]	FC-87	0.0128 –0.0204 m^3/m^2 · s	42–42.5	<0.6	5–90	7–50	68–90	——	——
1.0	Fig. 1a	[e]	1.0 × 2.0 cm^2	[f]	FC-72	0.0122 –0.0222 m^3/m^2 · s	28.5–62.5	<3.5	5–90	5–40	48–90	——	FC-72 with dissolved air had higher q''_{CHF}
1.0	Fig. 1a	[e]	1.0 × 2.0 cm^2	[f]	Water	0.0188 –0.0249 m^3/m^2 · s	67–72	3.0–14.1	5–500	2.5–58	No	——	——
1.0	Fig. 1a	[e]	1.0 × 2.0 cm^2	[f]	Methanol	0.0246 –0.0363 m^3/m^2 · s	38.9–69	2.7–13.7	25–490	5–60	250–490	——	——
						Lin et al. [22] (2004)							
1.0	Figs. 1b and 1c	[g]	2.54 × 7.6 cm^2	[f]	FC-72	0.505×10^{-3} -0.880×10^{-3} kg/s per nozzle	27–55	<6	10–60	8–38	30–60	$h\uparrow$ for Fig. 1c than for Fig. 1b; $q''_{CHF}\uparrow$ for Fig. 1c than for Fig. 1b	——

[a]Single, unconfined, pressure-atomized, uniform across center. [b]Pyrex block, ITO heater. [c]Low volume flux, no liquid flooding, just dropwise evaporation. [d]Cr-plated, Cu-block, cartridge heaters. [e]2 × 4 array, pressure-atomized, confined. [f]Cu-block, cartridge heaters. [g]4 × 12 array, pressure-atomized, confined.

Table 3 Summary of acceleration results from [6,18,23,24,47]

a, g	Orientation	Nozzle configuration	Heater size	Heater type	Working fluid	Flow rate/ volume flux	T_{sat}, °C	ΔT_{sc}, K	q'', W/cm^2	$T_s - T_{sat}$, K	q''_{CHF}, W/cm^2	Orientation/ acceleration trends	Comments
						Baysinger et al. [18] (2004)							
0.01, 1.0, 1.8	Figs. 1a and 1c	Single, partially confined, pressure-atomized	17 mm diam	Polycarbonate pedestal, ITO heater	FC-72	5.3 ml/s	N/A	N/A	0–20 W	N/A	No	No effect of change in accel reported	Recirculating closed-loop system in variable-acceleration environment
						Lin and Ponnappan [23] (2005)							
1.0	Figs. 1a–1c	[a]	2.54 × 7.6 cm^2	[b]	FC-72	N/A	27–55	<6	N/A	N/A	32–60	q''_{CHF} ↑ for Fig. 1c than for Fig. 1b; q''_{CHF} ↓ for Fig. 1a than for Fig. 1b	——
1.0	Fig. 1b	[a]	2.54 × 7.6 cm^2	Cu-block, plasma heater	Water	6.48×10^{-4} –9.0×10^{-4} kg/s per nozzle	63.5–90	2–37	100–500	12–43	350–500	h ↑ for b large heater, q''_{CHF} ↓ for Fig. 1b large heater than for a Fig. 1a small heater	——
						Golliher et al. [6] (2005)							
μ-g 1.0	Fig. 1a	Single, unconfined, air-atomized	3 in diam	Machined Al	Water	2.7–7.6 ml/s	N/A	N/A	N/A	N/A	N/A	Spray formed multiple separated segments of coalesced liquid on surface in microgravity	2.2 s drop tower, results not presented for heat transfer performance
						Rybicki and Mudawar [24] (2006)							
1.0	Fig. 1c	Single, pressure-atomized, unconfined (various nozzles)	1.0 × 1.0 cm^2	[b]	PF-5052	3.08–20.93 ml/s	50	12–27	10–237	$4 \leq T_s - T_{noz} \leq 50$ K	128–237	No effect of Fig. 1c or Fig. 1a on single-phase, nucleate boiling, or q''_{CHF} correlations	a from previous data with water, FC-72, FC-87
						Hunnel et al. [47] (2006)							
1.0	Figs. 1a and 1b	Single, partially confined, pressure-atomized	16 mm diam	Glass pedestal, TFR and ITO heaters	FC-72	4.8–9.8 ml/s	46.5–51.2	22.2–27.2	5–35	N/A	No	Little effect of orientation is reported	Reported that different orientations cannot simulate microgravity
1.0	Figs. 1a and 1b	Single, unconfined, pressure-atomized	16 mm diam	Glass pedestal, TFR and ITO heaters	FC-72	4.8–9.8 ml/s	46.5–51.2	22.2–27.2	5–35	N/A	No	T_s slightly ↓ for Fig. 1b than for Fig. 1a at 9.8 mL/s	——

[a]4 × 12 array, pressure-atomized, confined. [b]Cu-block, cartridge heaters.

Table 4 Summary of acceleration results from [19,31,44,46] and current research

a, g	Orientation	Nozzle configuration	Heater size	Heater type	Working fluid	Flow rate/ volume flux	T_{sat}, °C	ΔT_{sc}, K	q'', W/cm^2	$T_s - T_{sat}$, K	q''_{CHF}, W/cm^2	Orientation/ acceleration trends	Comments
						Yerkes et al. [19] (2006)							
0.01, 0.16, 0.36, 1.0, 1.8	Fig. 1a	Single, partially confined, pressure-atomized	16 mm diam	Glass pedestal, ITO heater	FC-72	5.26–10.5 ml/s	56	32.6	10.1–39.4	N/A	No	Nu ↑ for a ↓ ($\theta_s - \theta_{\infty,top}$ ↓ as a ↓)	Recirculating closed-loop system in variable-acceleration environment
						Gambaryan-Roisman et al. [31] (2007)							
0.05, 1.0, 1.8	Fig. 1a	Single, unconfined, pressure-atomized	20 mm diam	Convex surface, cartridge heaters	Water	0.25–0.5 l/ min	N/A	N/A	37.5–150 W	N/A	N/A	Temp. 5.1 mm below surface ↑ as a ↓ for flow above 0.4 l/ min	——
						Elston [44] (2009)							
0.01–2.02	Fig. 1a	4 × 4 nozzle array, confined, pressure-atomized	25.4× 25.4 mm^2	Phenolic base, TFR heater	FC-72	13.1–21.3 g/s	37.4–47.2	1.6–18.4	2.9–25	−10–35	22–25	ΔT_{sat} ↓ for a ↓; q''_{CHF} ↑ for a ↓; ΔT_{sat} changed less for high m, low ΔT_{sc}; trans. a trip q''_{CHF} prematurely	Recirculating closed-loop system in variable-acceleration environment
						Conrad et al. [46] (2009)							
0.01–1.8	Fig. 1d	Linear nozzle array, confined, pressure-atomized	25.4× 20.6 mm^2	Ohmite resistor	FC-72	0.775–3.86 l/ min	56	N/A	24.9–26.6	N/A	No	h slightly ↑ for a ↓	Reported lack of constant accel data; damage to array seal caused uncertainty and nonuniformity of flow
						Current research (2009)							
0.15–1.80	Fig. 1a	Single, partially confined, pressure-atomized	1.18× 1.18 cm^2	Glass pedestal, TFR heater	FC-72	6.18–8.94 ml/s	52.2–59.9	23.1–31.7	21.1–69.0	−15.4–20.3	No	ΔT_{sat} ↓ for a ↓; ΔT_{sat} ↓ for ΔT_{sc} ↑; ΔT_{sat} ↓ for V ↑	Recirculating closed-loop system in variable-acceleration environment

The objective of the present investigation was to continue the work presented by Baysinger et al. [18] and Yerkes et al. [19] to investigate the effects of variable gravity on the behavior of a partially confined, single-nozzle FC-72 spray, providing cooling for an upward-facing, horizontally oriented, heated surface. These previous reports described some of the first efforts using spray cooling as part of a recirculating closed-loop thermal management system in a variable-gravity environment. The main difference between these previous reports and the current research is the change from ITO to TFR heaters, which were able to provide higher heat fluxes for the spray-cooling research. FC-72 was chosen as the working fluid because it is nontoxic, nonflammable, and noncorrosive, and as a dielectric, it could be sprayed directly on the electrical component to be cooled (in this case, a TFR heater). FC-72 boils at approximately 56°C at atmospheric pressure [54], which allowed the fluid lines to be maintained at reasonable temperatures to avoid burn hazards. Further details on the properties of FC-72 are given by Geisler [55] and Michalak [56]. The experiment was again carried out using the NASA KC-135 to impose a variable-gravity environment. The behavior of the wall superheat, ΔT_{sat}, was examined by varying the following parameters: Heat flux to the spray, $21.1 \leq q''_{sp} \leq 69.0$ W/cm^2; acceleration field, $0.15 \leq a \leq 1.80$ g; coolant volumetric flow rate, $6.18 \leq V \leq 8.94$ ml/s; and coolant subcooling, $23.1 \leq \Delta T_{sc} \leq 31.7$ K. The heat fluxes tested in this effort were below q''_{CHF}, and the working fluid was estimated to have contained approximately 20–30% dissolved air as in [19], though the air content was not directly measured.

Experimental Design

The apparatus used in the current research was very similar to that described by Baysinger et al. [18], Baysinger [40], and Yerkes et al. [19]. The main differences were the addition of the TFR heater, which replaced the ITO heater, the addition of a drain loop to assist in clearing fluid from the chamber, and slight modifications to the working-fluid reservoir to improve flow rate stability during variable-gravity operation.

The experimental setup was designed to be essentially self-contained, so that it could be operated aboard the NASA Johnson Space Center Reduced-Gravity Research Aircraft. A structural and safety analysis was performed to ensure that the setup met the requirements imposed on experiments performed on this aircraft, and a test equipment data package was developed, following the guidance set out in various NASA documents [57–59]. The rig was constructed from T-slotted aluminum extrusions mounted onto an aluminum base plate which provided the primary interface between the test rig and the aircraft. Mounting holes around the perimeter of the base plate were used to securely bolt the test rig to the mounting points that were provided on the floor of the aircraft.

The experiment consisted of the fluid management and data acquisition systems, a test chamber which housed two opposing spray nozzles, and the heater pedestal assemblies. A photograph of this entire test rig can be found in Michalak [56]. A high-speed video setup was positioned to provide limited visualization of the spray system in operation.

The spray chamber (Fig. 2) was fabricated from standard vacuum components. The test space within the chamber was cylindrical, with a diameter of 14.6 cm and a length of 15.2 cm. The interior walls of the chamber were lined with several layers of mesh screen and steel wool to control the location of the fluid during variable-gravity operation. The outside of the cylindrical wall of the chamber was lined with copper tubing through which water could be pumped to control the temperature, and thus the pressure, inside the chamber. This chamber pressure P_{ch} was measured using a pressure transducer (Omega PX303-100A5V) and was used to calculate the saturation temperature within the test chamber. A triaxial linear servo accelerometer (Columbia Research Laboratories model SA-307HPTX) was mounted on the test chamber to provide acceleration data.

The test rig contained three flow loops: An FC-72 (nozzle) loop, a chamber drain loop, and a water loop (Fig. 3). The nozzle loop was

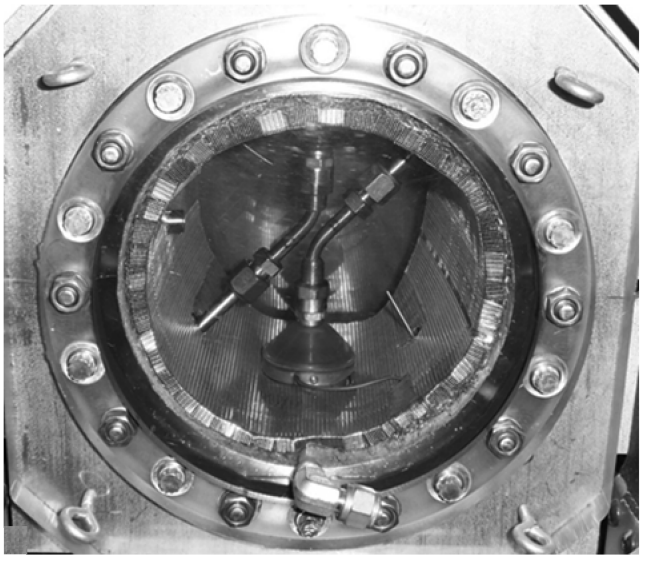

a)

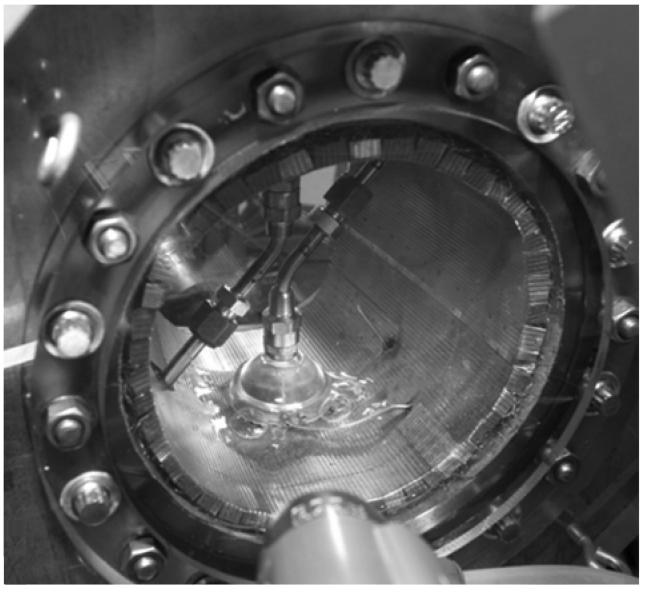

b)

Fig. 2 Photographs illustrating a) test chamber and b) test chamber during operation.

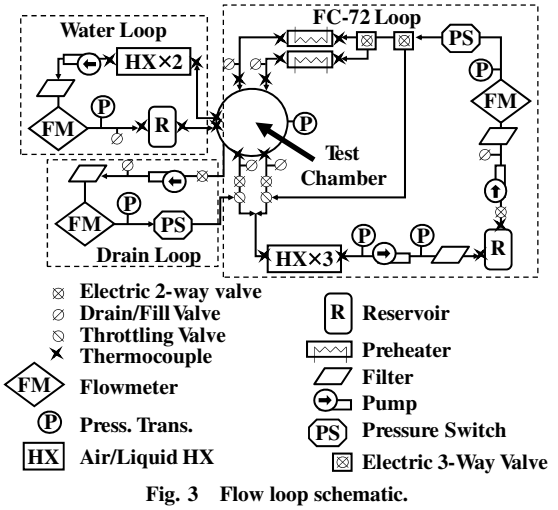

Fig. 3 Flow loop schematic.

used to deliver the working fluid, FC-72, through the spray nozzles and onto the heater surface. The bulk of the FC-72 inventory was stored in the reservoir, which was a custom-made stainless steel vessel with an internal stainless steel vane structure. A pad of copper wool was placed under this vane structure, and the suction line for drawing the working fluid out of the reservoir was placed in this copper wool, near the inside bottom corner of the reservoir. This arrangement was developed as an attempt to hold liquid near the suction line during variable-gravity operation using capillary forces. As will be discussed later, this reservoir met with limited success, and fluid management during some of the variable-gravity operation, especially the micogravity periods, was unsuccessful. Elston [41] and Elston et al. [43] provided further information on the evolution of the reservoir systems used on this test rig. The fluid was drawn out of the reservoir through an electrically controlled shutoff valve using a magnetically coupled gear pump and passed through a 40 μm filter to prevent clogging of the nozzles.

After the filter, the fluid passed through a flow meter (Sponsler MF90CBPHA4X-V Lo-Flo Series flowmeter with an SP711-3 three-wire analog transmitter), followed by a pressure transducer (Omega PX303-200A5V) and a pressure switch, which was set to shut down the power to the flow loops and heaters in the event of an overpressure situation. The fluid then passed to a series of electrically controlled three-way valves. The first valve could be set to either send the fluid to the nozzles in the chamber or, if necessary, bypass the chamber. The next valve was used to select whether the fluid would be sprayed through the top or bottom nozzle. For this set of research, only the nozzle spraying on the upward-facing horizontal heater surface was used. After the three-way valves, the fluid passed through a preheater, which consisted of a length of copper tubing wrapped with a heater tape and insulation, controlled by a proportional–integral–derivative temperature controller (Fuji Electric PXV3-TBY2-5V). This was used to control the temperature of the fluid entering the nozzle. After the preheaters, the fluid was sprayed through the nozzle and onto the heater surface inside the chamber. The nozzle used in this testing (FullJet 1 from Spraying Systems Company) was the same as that described by Baysinger et al. [18] and Yerkes et al. [19]. This nozzle had a nominal orifice diameter of 0.79 mm and was positioned approximately 1 cm from the heated surface, aligned axially with the heater post. For this nozzle, as configured in the experiment, a pressure drop of approximately 352 kPa corresponded to a volumetric flow rate of approximately 9.0 ml/s, and a pressure drop of approximately 207 kPa corresponded to a volumetric flow rate of 6.7 ml/s. The fluid was collected in the sump structure and removed from the chamber.

Once it left the chamber, the fluid passed through a shutoff valve and into a series of three liquid/air heat exchangers. These heat exchangers condensed and subcooled the working fluid so that there was less chance of vapor being passed through the pumps or into the reservoir. The working fluid then passed through a pressure transducer (Omega PX303-100A5V), a magnetically coupled gear pump, another pressure transducer (Omega PX303-200A5V), and another 40 μm filter before being returned to the reservoir. The two pumps were arranged in this configuration to provide a push/pull effect on the chamber to attempt to provide better control of the fluid spray and inventory. Type-E thermocouples (0.16 cm diameter) were placed at strategic locations around the flow loop and in the test chamber to monitor temperatures. Throughout this experiment, type-E thermocouples were used, due to their higher sensitivity in the temperature range of interest.

A second loop was used for draining the chamber, if the sumps were unable to remove sufficient fluid during the variable-gravity operation. A fitting was installed near the bottom of the front faceplate of the chamber. If the chamber began to fill with excess working fluid, the drain loop would remove the fluid directly from the chamber to attempt to keep the chamber fluid level below the heater surface and to maintain adequate flow of liquid back to the reservoir.

The water loop was used to control the temperature and pressure inside the chamber. The temperature of the water that was circulated through the coil around the chamber was not actively controlled. The water stayed near the ambient temperature and cooled the walls of the chamber, so that vapor that contacted the walls would condense back to liquid for removal from the chamber.

The heater used was similar to the heater/pedestal assembly described by Yerkes et al. [19] with a TFR heater instead of an ITO heater. Representative photographs of a pedestal and TFR heater are given in Fig. 4. The light-colored regions on the sides of the darker-colored heater in Fig. 4b are the regions of the conductive epoxy that was used to connect the copper leads to the heater to provide power to the heater. The heater had an area of $A = (1.18 \pm 0.0127) \times (1.18 \pm 0.0127)$ cm^2. The cylindrical pedestals consisted of several layers. The first three layers comprised the TFR heater and were investigated by Glaspell [48]. Table 5 summarizes the sizes and thermal conductivities of the thin heater layers, which included a glass cover plate, a resistive layer, and a ceramic substrate. Michalak [56] presents a schematic to clarify the heater geometry. This schematic includes the heat rates and a qualitative representation of the temperature profile expected through the heater.

The heater layers, with the thin ceramic substrate at the bottom, rested on two thin, stacked wafers of glass which were each 0.001 m thick. These glass layers sat on top of a glass pedestal, which had a thermal conductivity of approximately 1.04 W/m-K. This glass pedestal supported and insulated the heater, in an attempt to minimize heat loss through the heater support. A small type-E thermocouple (0.0254 cm diameter) was embedded between the heater substrate and the first glass layer to measure the interface temperature, T_{int}. The surface temperature could not be measured directly without interfering with the behavior of the spray, so T_s was calculated from T_{int} using a one-dimensional conduction model. As the layers that composed the heater geometry for the TFR were very similar to those presented by Elston et al. [41,44], Puterbaugh et al. [16,17], Glaspell [48], and Kreitzer [49], the T_s calculation is similar

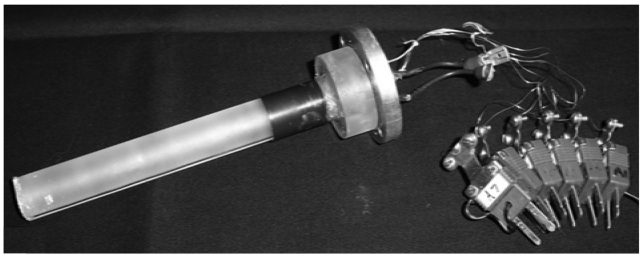

a)

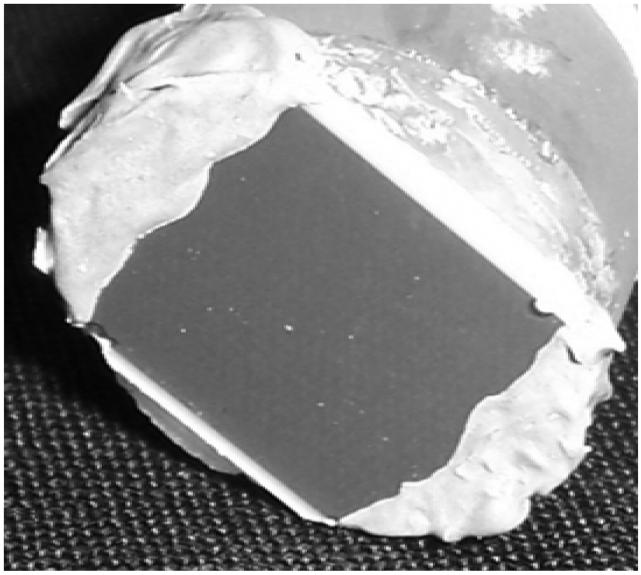

b)

Fig. 4 Photographs detailing a) entire pedestal and b) close-up of TFR heater.

Table 5 Heater-layer dimensions and thermal conductivities [48]

Layer	Thickness, mm	Thermal conductivity, W/m-K
Ceramic substrate	$H_{sub} = 0.634 \pm 0.010$	$k_{sub} = 27.0$
Heater	$H_{htr} = 0.008 \pm 0.002$	$k_{htr} = 1.04$
Glass cover	$H_{cov} = 0.040 \pm 0.005$	$k_{cov} = 1.04$

to that presented by those researchers. The details of this calculation are presented in Michalak [56] and the resulting expression for T_s is

$$T_s = T_{int} + \frac{q}{A}\left[\frac{H_{sub}}{k_{sub}}f + \frac{H_{htr}}{k_{htr}}\left(f - \frac{1}{2}\right) + \frac{H_{cov}}{k_{cov}}(f-1)\right] \quad (1)$$

Six 0.0254 cm diameter thermocouples were also embedded between the glass layers, as shown by Yerkes et al. [19]. The results of Baysinger et al. [18], based on a comparison of a transient analytical calculation to experimental data, estimated a heat loss down a polycarbonate pedestal to be approximately $f = 1\%$. Baysinger [40] compared several different numerical solutions to estimate f and determined the range to be $1 \leq f \leq 2.5\%$. Yerkes el al. [19] compared numerical solutions to an analytical solution and verified this range for f. The results of Baysinger [40] and Yerkes et al. [19] suggest a slightly higher loss down the pedestal than the original estimate from Baysinger et al. [18]. Since the majority of the data presented by Yerkes et al. [19] can be seen to be contained within $f = 1.5 \pm 0.5\%$, this value is used as the percentage of heat lost down the pedestal for the present configuration, which had a very similar geometry to that examined previously. A temperature limit/alarm switch module (Love Controls model 1290 dual alarm) was used to limit the heater temperature to protect the heater from overtemperature conditions ($T_{int} \leq 100°C$).

The pedestal was surrounded by an annular sump structure fitted with a containment cap, as shown schematically in Fig. 5a [19], with the cap shown exploded from the rest of the sump for clarity. This structure served both as fluid containment and as a means of removing the fluid from the chamber. The nozzle was positioned just outside the opening in the top of the cap. A photograph of the nozzle placement over the cap is shown in Fig. 5b. During operation, some of the liquid bounced off the surface of the heater. The cap was able to direct the majority of this fluid back down into the annular region formed by the walls of the sump and the sides of the heater pedestal, so that it would not float around in the large volume of the test chamber during variable-gravity operation. However, it can be seen in Fig. 5b that the fluid tended to stick to any surface that it contacted, and there was some surface tension flow around the nozzles. This behavior is similar to that reported by Baysinger et al. [18]. The gap formed between the cap and the nozzle would allow any vapor that was generated on the heater surface to escape into the test chamber, where it could condense on the chamber walls. The slots machined into the top of the sump allowed liquid to enter the sump from the test chamber. These slots also allowed fluid to enter the test chamber from the sump, if the sump annulus became too full, so that the heater surface would not become flooded. This configuration prevented the entire region around and above the heater from being completely filled with liquid, as would be the case in a fully confined spray system. However, it could allow some of the fluid to bounce back onto the heater surface from the walls of the sump and cap, so it is not a fully unconfined system. Therefore, this configuration is referred to as partially confined.

Two type-E thermocouples (0.16 cm diameter) were positioned inside the sump annulus to monitor the temperature of the fluid that exited the heater. One thermocouple, measuring the upper film temperature T_{uf}, was placed just off the surface of the heater, and a second, measuring the lower film temperature T_{lf}, was about 1.2 cm down from the upper film temperature, near the side of the glass pedestal. The nozzle inlet temperature T_{noz} was also measured using the same type of thermocouple.

The thermocouples in and around the pedestal in the test chamber were all referenced through a dry-well ice point (HART Scientific 9101) to improve the stability and accuracy of the temperature readings. Additionally, these thermocouples were calibrated using an oil-bath/RTD (resistance temperature detector) calibration setup (Hart Scientific model 5628 RTD with a model 1502A readout). Details of this calibration are presented by Michalak [56].

The heater power was measured using two different voltage measurements. The first was across the heater film itself, E_H, as close to the heater as possible to minimize voltage error from the heater leads. The second voltage measurement, E_R, was measured across a precision resistor, which had a nominal resistance of $R_p = 0.1\Omega$ at 25°C. The heater power is given by

$$q = E_H * \frac{E_R}{R_p} \quad (2)$$

The data presented here consisted of three flights of about 40 parabolas each. Each parabola provided approximately 35 s of elevated gravity, at approximately $a = 1.8$ g, followed by about 25 s of reduced gravity. The level of the acceleration for the reduced-gravity portion of the parabola was set by the pilots flying the aircraft, depending on the flight trajectory followed. The data being taken

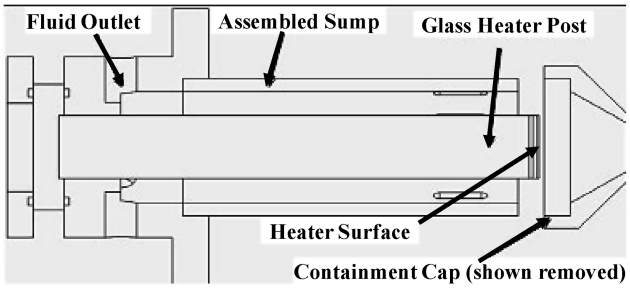

a)

b)

Fig. 5 Illustrations clarifying a) schematic of pedestal in sump and cap [19] and b) close-up photograph of nozzle/cap positioning, as well as surface tension flow during operation.

Table 6 Instrument/calibration uncertainties

Measurement	Calibration uncertainty
P_{ch}	0.25 psia
a	0.03 g
V	0.413 ml/s
E_H	$(0.000045 \times E_H + 0.0006)$ V
E_R	$(0.000040 \times E_R + 0.000007)$ V
R_p	0.00002Ω
T_{int}	0.054°C
T_{lf}	0.065°C
T_{uf}	0.065°C
T_{noz}	0.061°C

were observed to come to steady state within approximately 5 s, so the 25 s reduced-gravity period was sufficient to collect steady-state values.

Data were routed through a data acquisition system (Agilent 34970A data acquisition/switch unit with Agilent 34901A multiplexer modules) to a laptop computer. An analysis was carried out to estimate the uncertainties associated with the computed values. First, the uncertainties in the measured values were identified and quantified. The uncertainty values presented in Table 6 are the fixed uncertainties associated with the accuracy and calibration of the measuring devices. To determine the uncertainty in the measured values, the device uncertainty was then added to the confidence interval for each averaged measurement, as described by Montgomery and Runger [60]. The uncertainties in the calculated values could then be determined by propagating these measurement uncertainties through the method outlined by Fox and McDonald [61]. Details of these uncertainty estimate calculations are given by Michalak [56].

The fluid loop was filled before the first flight, and some air was allowed to bleed back into the system, so that the air content of the FC-72 was estimated to be 20–30% by volume, as discussed by Yerkes et al. [19]. Running the experiment with air dissolved in the FC-72 allowed for the system pressure to be close to ambient, which increased the saturation temperature in the chamber and allowed for modifications or repairs to the rig without fully pumping down the system. For this research, the dissolved air content of the working fluid was being controlled by maintaining a saturation pressure range in the system. No fluid samples were collected or analyzed to measure air content, due to the complexity of obtaining the working-fluid samples for analysis while at the NASA facilities.

Results and Discussion

The objective of this experiment was to determine the behavior of the wall superheat in a thermal management system using spray cooling with a single nozzle in a recirculating closed loop when subjected to a variable-gravity environment. The dependence of ΔT_{sat} on heat flux, acceleration, subcooling, and flow rate was examined.

To determine the behavior of this system, the flow rate and level of subcooling were set at the beginning of each flight and were maintained for the duration of that flight. The heater power and the acceleration were then varied. Each heat input level was maintained for at least one full parabola, which consisted of an elevated-gravity period followed by a reduced-gravity period. The acceleration (gravity) reported here is the portion of the total acceleration vector which is normal to the upward-facing, horizontally oriented heater surface. After at least one full parabola, the heater input power was adjusted to the next desired level: generally, in steps of 2 to 5 W. In some cases, the same heater power was maintained for several parabolas. Data were collected by the data acquisition system approximately once every 2 s. To reduce the data, the transient portions, such as those during major acceleration transients, heater power adjustments, or adverse flow rate excursions, were discarded. The remaining data were divided between 10 separate cases, each of which consisted of a constant flow rate, subcooling, and acceleration. The only parameter that was varied in each case was the heat input.

Table 7 Parameters for 10 cases tested during flights

Case	a, g	T_{sat}, °C	ΔT_{sc}, K	V, ml/s
		Flight 1		
1	0.15 ± 0.03	53.8 ± 1.2	25.4 ± 1.3	8.70 ± 0.45
2	1.04 ± 0.04	53.8 ± 1.1	25.1 ± 1.1	8.64 ± 0.43
3	1.78 ± 0.03	53.6 ± 1.2	24.8 ± 1.2	8.73 ± 0.43
		Flight 2		
4	0.37 ± 0.04	59.5 ± 1.0	30.7 ± 1.0	8.63 ± 0.43
5	1.06 ± 0.04	59.1 ± 1.0	30.0 ± 1.0	8.70 ± 0.42
6	1.78 ± 0.03	59.3 ± 1.0	30.3 ± 1.0	8.61 ± 0.42
		Flight 3		
7	0.16 ± 0.04	58.9 ± 1.1	30.0 ± 1.1	6.55 ± 0.45
8	0.36 ± 0.04	59.2 ± 1.0	30.3 ± 1.0	6.58 ± 0.44
9	1.06 ± 0.04	58.4 ± 1.0	29.1 ± 1.0	6.61 ± 0.42
10	1.76 ± 0.03	58.8 ± 1.0	29.3 ± 1.0	6.43 ± 0.42

Table 7 shows the 10 various cases that were identified for these three flights.

Two representative samples of transient data collected during the flight tests are shown in Fig. 6, which demonstrate how quickly the system was able to reach steady state after a change to one of the parameters, even during the short duration of each parabola. A sample of data collected during flight 1, consisting of three parabolas, is presented in Fig. 6a. Initially, the heat flux was $q''_{sp} = 26.8$ W/cm^2 and the acceleration was $a = 1.8$ g. At time A, the pilot initiated a reduced-gravity event, which rapidly reduced the acceleration to $a = 0.15$ g. Following this acceleration drop, the interface temperature decreased by 2°C to $T_{int} = 57.7$°C. At time B, the acceleration returned to $a = 1.8$ g and the interface temperature returned to $T_{int} = 59.7$°C. During this acceleration event, both the volumetric flow rate and the heater power remained relatively constant. At time C, another reduced-gravity event was initiated, in which the acceleration was reduced to $a = 0.01$ g. Once again,

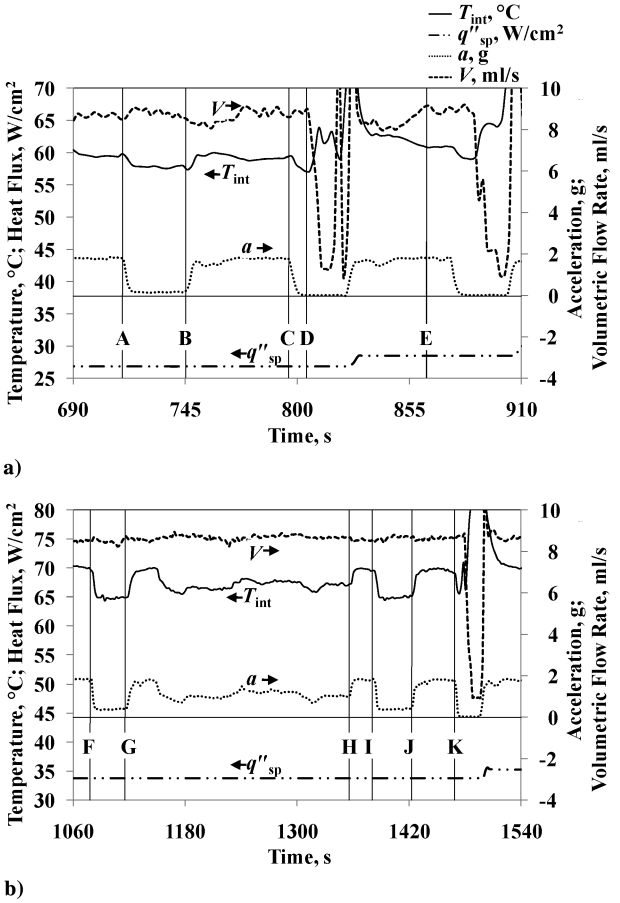

Fig. 6 Representative transient data traces: a) flight 1 and b) flight 2.

though the flow rate and heater power initially remained relatively constant, the interface temperature dropped from $T_{int} = 59.4$ to 57.2°C. However, at time D, the volumetric flow rate dropped dramatically from $V = 8.6$ to 1.5 ml/s, due to the pump drawing vapor from the reservoir as the liquid floated away from the suction tube, despite the vane structure and copper wool. This caused a predictable spike in the interface temperature as the flow of cooling fluid to the heater was interrupted. Between times D and E, the flow rate was still fluctuating and the heat flux was increased to $q''_{sp} = 28.4$ W/cm^2. After time E, the flow rate became relatively stable at $V = 8.8$ ml/s and the interface temperature stabilized at approximately $T_{int} = 61$°C, which was consistent with the higher heat input. At the onset of the next reduced-gravity event, the temperature dropped to $T_{int} = 59$°C before climbing rapidly following another interruption in the coolant flow rate.

A similar sample of data, collected during flight 2 and consisting of three parabolas and a nominal 1-g turn, is presented in Fig. 6b. At the beginning of this period, the heat flux was $q''_{sp} = 33.7$ W/cm^2, the acceleration was $a = 1.8$ g, and the interface temperature was $T_{int} = 70$°C. At time F, the acceleration dropped to $a = 0.35$ g. Though the flow rate did not change, the interface temperature dropped to $T_{int} = 65$°C. At time G, the acceleration returned to $a = 1.8$ g and the interface temperature climbed to $T_{int} = 70$°C. After this elevated-gravity period, the aircraft entered a turn period, during which the acceleration was $a = 1.0$ g. Over the course of this turn, V and q''_{sp} remained stable while the acceleration experienced several small variations. The variation in T_{int} was observed to closely follow the changes in acceleration. At point H, the aircraft entered another elevated-gravity period, with an acceleration change to $a =$ 1.8 g and a corresponding step in interface temperature to $T_{int} = 70$°C. From I to J, the acceleration dropped to $a = 0.36$ g, with a temperature drop to $T_{int} = 65$°C. After this reduced-gravity period, the temperature returned to $T_{int} = 70$°C. At time K, the aircraft entered a reduced-gravity period, with $a = 0.01$ g. As in Fig. 6a, the transition to microgravity was followed by a drastic reduction in the flow rate. After the acceleration was reduced the interface temperature was observed to drop to $T_{int} = 65.6$°C before increasing rapidly following the flow rate interruption.

At acceleration levels in the microgravity range ($a \leq 0.01$ g), the flow rate was consistently interrupted due to vapor being pulled into the pump from the reservoir. While this prevented the collection of steady-state data at this acceleration, it became clear from the behavior of T_{int} that a disruption of coolant flow, even for a short period of time, can have potentially catastrophic consequences for a thermal management system employing spray cooling. Care must be taken when considering such systems to ensure that the design is robust enough to maintain the required coolant flow rates throughout the entire anticipated operating range.

The wall superheat versus acceleration for the three different flights is portrayed in Fig. 7. Within each flight, the flow rate and subcooling remained constant, and each individual curve represents a different heat flux. It should be noted that these curves are plotted as linear fits to the data to aid in labeling and visualization. The intent is not to imply that there is actually a linear relationship between acceleration and wall superheat. All of the curves plotted in Fig. 7 were observed to have a slightly positive slope, which indicated that for a given heat flux, decreasing acceleration corresponded to decreasing wall superheat. One possible explanation for the decrease in surface temperature in reduced gravity is that when the body forces are reduced, the impacting droplets can more easily splash the heated liquid film up and away from the surface, so that cooler incoming fluid can more easily approach the surface, providing increased cooling. This trend is similar to that reported by Elston [44], Yerkes et al. [19], Conrad et al. [46], and some of the results from Sone et al. [28]. Other portions of Sone et al. [28], Yoshida et al. [29], and Gambaryan-Roisman et al. [31] noted an increase in temperature subsequent to a decrease in acceleration.

The effect of subcooling on the wall superheat is illustrated in Fig. 8. In each of these plots, the acceleration and flow rate were held constant. All of the curves had a negative slope, which indicated that

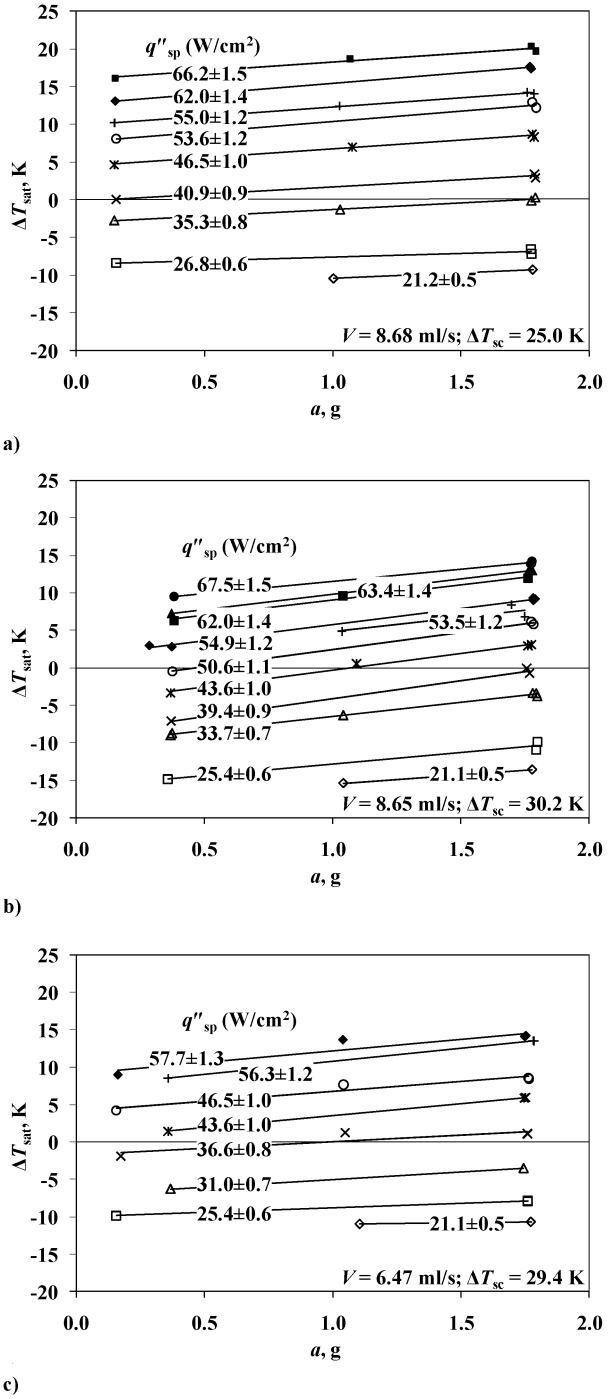

Fig. 7 Effect of acceleration on wall superheat: a) flight 1 ($V = 8.68 \pm 0.42$ ml/s, $\Delta T_{sc} = 25.0 \pm 1.1$ K, and $T_{sat} = 53.7 \pm 1.1$°C); b) flight 2 ($V = 8.65 \pm 0.43$ ml/s, $\Delta T_{sc} = 30.2 \pm 1.0$ K, and $T_{sat} = 59.3 \pm 1.0$°C); and c) flight 3 ($V = 6.47 \pm 0.44$ ml/s, $\Delta T_{sc} = 29.4 \pm 1.0$ K, and $T_{sat} = 58.8 \pm 1.0$°C).

for a given heat load the wall superheat was lower when there were higher values of coolant subcooling. A similar trend was reported by Elston [44], Pais et al. [11], and Chow et al. [3]. The slopes in Fig. 8a ($a = 1.05$ g) were slightly steeper than those in Fig. 8b ($a = 1.78$ g). In each plot, the slopes remained relatively constant throughout the range of heat fluxes plotted, which was contrary to the results observed by Elston [44]. For that multiple-nozzle experiment, the subcooling dependence was noted throughout the reduced-gravity testing. In the elevated-gravity testing, the wall superheat was found to decrease with increasing subcooling for low heat fluxes, but at higher heat fluxes, there was no noted effect of subcooling on the wall superheat. This change in behavior at different heat fluxes was not observed in the current experiment, which used a single nozzle.

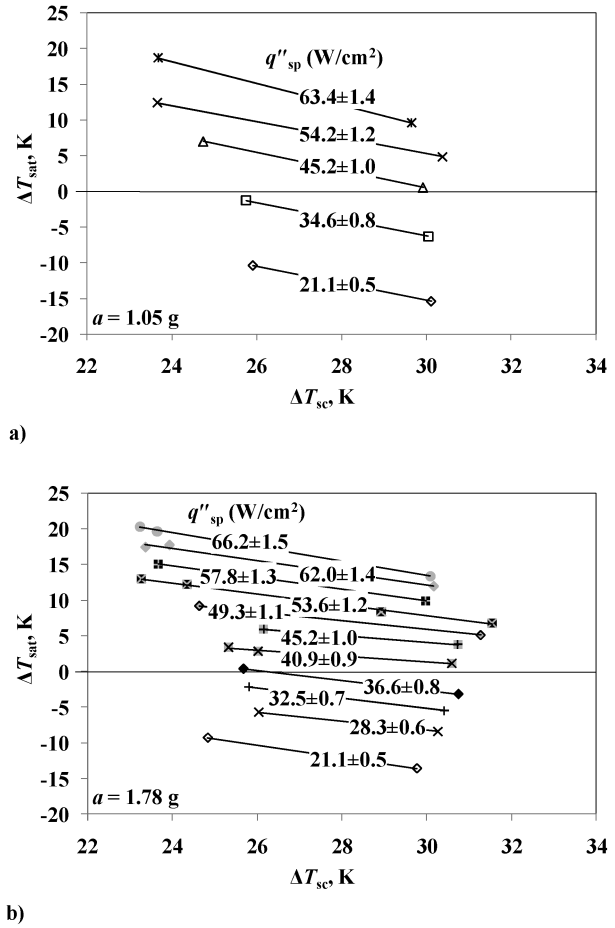

Fig. 8 Effect of subcooling on wall superheat ($V = 8.66 \pm 0.42$ ml/s): a) $a = 1.05 \pm 0.04$ g and b) $a = 1.78 \pm 0.03$ g.

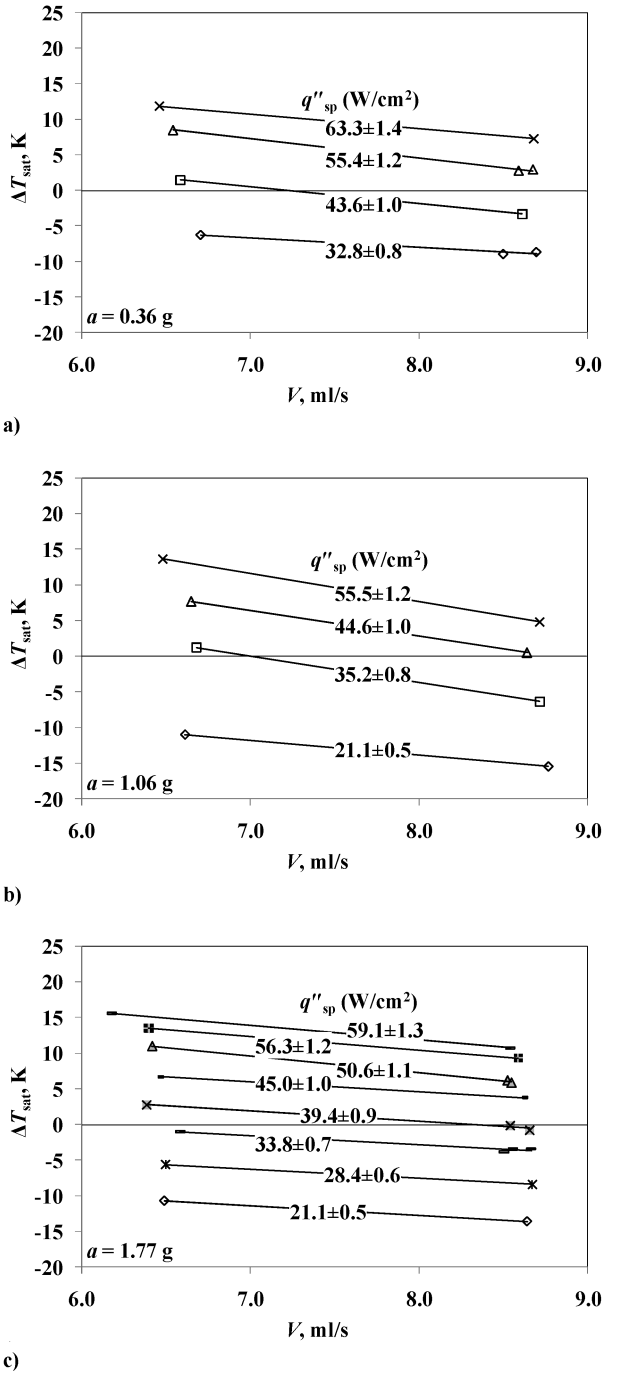

Fig. 9 Effect of flow rate on wall superheat ($\Delta T_{sc} = 29.9 \pm 1.5$ K): a) $a = 0.36 \pm 0.04$ g and b) $a = 1.06 \pm 0.04$ g; and c) $a = 1.77 \pm 0.04$ g.

The effect of volumetric flow rate on wall superheat for three different acceleration levels can be seen in Fig. 9. In each plot, the subcooling and acceleration levels were kept constant. For each heat flux, the wall superheat was lower for higher values of volumetric flow rate, which was true for all acceleration levels. This trend was similar to that observed by Yoshida et al. [29], Hunnel et al. [47], Kim [2], Mudawar [1], and Estes and Mudawar [12]. Elston [44] noted this trend, but also reported that at higher flow rates in reduced gravity, there was a drastic increase in wall superheat, which was not noted in the present research. This altered behavior was likely due to the differences between single-nozzle and multiple-nozzle spray systems. There are no spray-to-spray interactions in a single-nozzle system, so fluid may be less likely to build up on the surface at higher flow rates.

The heat transfer characteristics for flight 1, consisting of cases 1, 2, and 3, are given in Fig. 10a. The left-hand side of the plot (with the q''_{sp} axis, $\Delta T_{sat} = T_s - T_{sat} = 0$, as the separating line) is referred to as the single-phase region, and the right-hand side of the plot is the two-phase region. For visualization purposes, linear trend lines were applied to the single-phase and two-phase regions separately. For all three cases, ΔT_{sat} increased with increasing heat flux, as would be expected. For case 1, with the lowest value of a, ΔT_{sat} for any given heat flux was less than that for case 2 or case 3. From Table 7, the difference between the average values of V for these three cases was less than 3%, and the average ΔT_{sc} and T_{sat} values varied by only approximately 2%. Therefore, the acceleration was the primary difference between the parameters for cases 1, 2, and 3. There was a ΔT_{sat} shift between cases 2 and 3, but it was not as pronounced as that between cases 1 and 2. Thus, between $a = 0.15$ and 1.04 g, there was a large change in ΔT_{sat} for a given q''_{sp}, but for between $a = 1.04$ and 1.78 g there was much less change. Another point to note is that for Fig. 10a there was very little difference between the slopes of the single-phase and two-phase regions. The data appeared to be nearly linear throughout the entire range of ΔT_{sat}. Also, the curves were relatively parallel. There may have been a small amount of divergence as ΔT_{sat} increased, but the slopes of these cases were approximately the same. This is similar to the results presented by Estes and Mudawar [12], in which no significant change in slope was reported through the nucleate boiling region. Therefore, it is difficult to determine how much of the heat transfer for the present research was due to single-phase convection and how much was due to boiling.

The data for flight 2, consisting of cases 4, 5, and 6, are shown in Fig. 10b. In this data set, there were small differences between the slopes of the single-phase and two-phase regions. When viewing the three different cases plotted in Fig. 10b, there was again a shift in the ΔT_{sat} data. For case 4 ($a = 0.37$ g), the wall superheat was smaller at a given heat flux when compared to case 5 ($a = 1.06$ g).

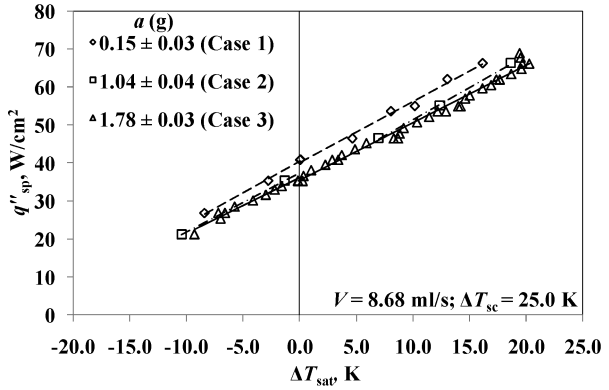

a)

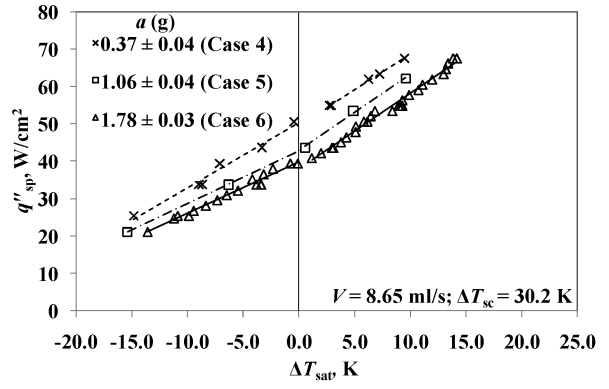

b)

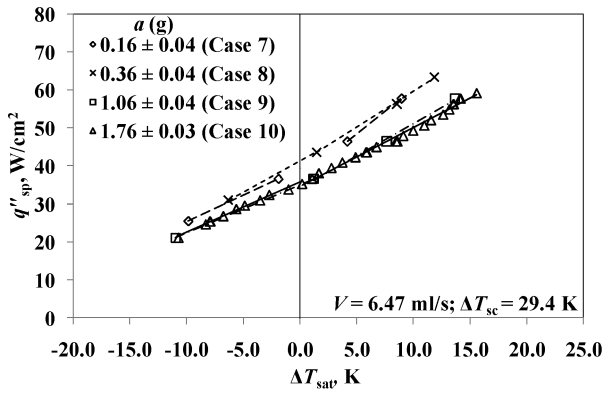

c)

Fig. 10 Heat flux to spray versus wall superheat: a) flight 1 ($V = 8.68 \pm 0.42$ ml/s, $\Delta T_{sc} = 25.0 \pm 1.1$ K, and $T_{sat} = 53.7 \pm 1.1$°C); b) flight 2 ($V = 8.65 \pm 0.43$ ml/s, $\Delta T_{sc} = 30.2 \pm 1.0$ K, and $T_{sat} = 59.3 \pm 1.0$°C); and c) flight 3 ($V = 6.47 \pm 0.44$ ml/s, $\Delta T_{sc} = 29.4 \pm 1.0$ K, and $T_{sat} = 58.8 \pm 1.0$°C).

However, there was also a larger shift toward increasing ΔT_{sat} between case 5 and case 6 ($a = 1.78$ g) than was noted between cases 2 and 3 in Fig. 10a.

The data from flight 3 (cases 7, 8, 9, and 10), are presented in Fig. 10c. There was little difference between the two reduced-acceleration cases (case 7, at $a = 0.16$ g, and case 8, at $a = 0.36$ g). There was also little difference between case 9 ($a = 1.06$ g) and case 10 ($a = 1.76$ g). There was still a downward shift in the ΔT_{sat} values for the reduced-gravity cases (7 and 8) compared to the higher-gravity cases (9 and 10). In Fig. 10c, however, there was some divergence between cases 7 and 8 and cases 9 and 10 as q''_{sp} increased, which indicated that the change in the wall superheat with a change in acceleration is greater at higher heat fluxes.

Comparing Fig. 10a (flight 1) to Fig. 10b (flight 2) can give insight into the effect of subcooling on the acceleration dependency for the system behavior. There is a negligible difference in the flow rates between these two flights. In contrast, the subcooling temperature for flight 1 was $\Delta T_{sc} = 25.0$ K, while the subcooling temperature for flight 2 was $\Delta T_{sc} = 30.2$ K. In Fig. 10b, the curves are spread further apart than in Fig. 10a, as mentioned above. In other words, the reduction in the wall superheat due to a reduction in acceleration was more pronounced in the cases with the higher subcooling. This suggested a coupled effect of acceleration and subcooling temperature for this spray-cooling system configuration, with higher subcooling levels actually enhancing the observed behavior dependence on acceleration. A similar coupling of acceleration and subcooling was reported by Elston [44], who noted that as the subcooling temperature decreased, the q''_{sp} versus ΔT_{sat} curves for the reduced-gravity cases approach those of the elevated-gravity cases.

Comparing Figs. 10b and 10c , the effect that varying the flow rate has on the spray-cooling behavior can be examined. In both, there is a good deal of separation between the low-acceleration curves and the higher-acceleration curves. However, in Fig. 10b, the curves are all relatively parallel, especially in the two-phase region. On Fig. 10c, it appears that the lines are much less parallel, especially on the two-phase half of the curve. This means that in flight 3 there was a higher heat transfer coefficient in the lower accelerations, since the slope of these curves is an indication of the convective/boiling heat transfer coefficient. The higher flow rate may tend to mask some of the dependence of the heat transfer coefficient on acceleration in the two-phase region. In all three parts of Fig. 10, the slope in the single-phase region was slightly higher for the lower accelerations, which explains why there was such a temperature difference between the lower-acceleration curves and the higher-acceleration curves. It was only in Fig. 10c, with the lower flow rate, that this larger slope carried over into the two-phase region.

In the open literature, researchers have presented data on plots showing heat flux versus T_s, heat flux versus $T_s - T_{noz}$ or $T_s - T_f$, or in nondimensional terms. Several of these alternative presentations were explored for this data set. However, it was determined that little additional insight could be gained from these methods of showing this particular data. Several of these alternate methods can be seen in Michalak [56].

Conclusions

The effects of variable gravity on the cooling performance of a partially confined FC-72 spray, in a closed-loop, recirculating system, were investigated. A test rig, which had been previously flown on NASA's reduced-gravity testing aircraft, was modified to test higher heat fluxes and provide a more stable flow rate. Along with the effects of acceleration, the effects of varying the coolant subcooling and the volumetric flow rate were also investigated. The wall superheat was observed to increase as the heat input was increased, as expected. For a given heat flux, the wall superheat decreased more in the reduced-gravity cases compared to the normal- or elevated-gravity cases. The normal-gravity cases tended to have a slightly lower wall superheat than the elevated-gravity cases for a given heat flux. The wall superheat tended to be lower for cases with a higher subcooling. Higher values of coolant subcooling were also observed to enhance the effect of acceleration, as the difference in wall superheat in reduced gravity was more significant for the cases with higher subcooling. The wall superheat decreased with higher volumetric flow rates. It was found that care must be exercised when designing thermal management systems for variable-gravity environments, to ensure that the system design is robust enough to maintain the necessary flow rates throughout the anticipated operating range, since even a momentary interruption in coolant flow can lead to a dramatic and potentially catastrophic temperature increase in the device being cooled.

Acknowledgments

This research was conducted as a collaborative effort with the NASA John H. Glenn Research Center (GRC) at Lewis Field using

the blanket interagency agreement SAA3-307 between GRC and the U.S. Air Force Research Laboratory, Order No. 12.

References

[1] Mudawar, I., "Assessment of High-Heat-Flux Thermal Management Schemes," *IEEE Transactions on Components and Packaging Technologies*, Vol. 24, No. 2, June 2001, pp. 122–141. doi:10.1109/6144.926375

[2] Kim, J., "Spray Cooling Heat Transfer: The State of the Art," *International Journal of Heat and Fluid Flow*, Vol. 28, No. 4, Aug. 2007, pp. 753–767. doi:10.1016/j.ijheatfluidflow.2006.09.003

[3] Chow, L. C., Sehmbey, M. S., and Pais, M. R., "Critical Heat Flux in Spray Cooling," 34th AIAA Aerospace Sciences Meeting and Exhibit, AIAA Paper 96-0727, Reno, NV, Jan. 1996.

[4] Rini, D. P., Chen, R., and Chow, L. C., "Bubble Behavior and Nucleate Boiling Heat Transfer in Saturated FC-72 Spray Cooling," *Journal of Heat Transfer*, Vol. 124, No. 1, Feb. 2002, pp. 63–72. doi:10.1115/1.1418365

[5] Kim, J., "Review of Reduced Gravity Boiling Heat Transfer: US Research," *Journal of the Japan Society of Microgravity Applications*, Vol. 20, No. 4, 2003, pp. 264–271.

[6] Golliher, E. L., Zivich, C. P., and Yao, S. C., "Exploration of Unsteady Spray Cooling for High Power Electronics in Microgravity Using NASA Glenn's Drop Tower," 2005 ASME Summer Heat Transfer Conference, American Society of Mechanical Engineers Paper HT2005-72123, San Francisco, July 2005.

[7] Silk, E. A., Golliher, E. L., and Selvam, R. P., "Spray Cooling Heat Transfer: Technology Overview and Assessment of Future Challenges for Micro-Gravity Application," *Energy Conversion and Management*, Vol. 49, No. 3, 2008, pp. 453–468. doi:10.1016/j.enconman.2007.07.046

[8] Sehmbey, M. S., Chow, L. C., Pais, M. R., and Mahefkey, T., "High Heat Flux Spray Cooling of Electronics," *Proceedings of the 12th Symposium on Space Nuclear Power and Propulsion*, Vol. 324, AIP Conference Proceedings, American Inst. of Physics, Melville, NY, Jan. 1995, pp. 903–909. doi:10.1063/1.47084

[9] Cader, T., and Tilton, D., "Implementing Spray Cooling Thermal Management in High Heat Flux Applications," *ITHERM '04: 9th Intersociety Conference on Thermal and Thermomechanical Phenomena in Electronic Systems*, Vol. 2, Inst. of Electrical and Electronics Engineers, Piscataway, NJ, June 2004, pp. 699–701. doi:10.1109/ITHERM.2004.1318358

[10] Tilton, D. E., Chow, L. C., and Mahefkey, E. T., "High Power Density Evaporative Cooling," *22nd AIAA Thermophysics Conference*, AIAA Paper 87-1536, AIAA, Honolulu, HI, June 1987.

[11] Pais, M., Tilton, D., Chow, L., and Mahefky, E., "High Heat Flux, Low Superheat Evaporative Spray Cooling," 27th AIAA Aerospace Sciences Meeting, AIAA Paper 89-0241, Reno, NV, Jan. 1989.

[12] Estes, K., and Mudawar, I., "Correlation of Sauter Mean Diameter and Critical Heat Flux for Spray Cooling of Small Surfaces," *International Journal of Heat and Mass Transfer*, Vol. 38, No. 16, 1995, pp. 2985–2996. doi:10.1016/0017-9310(95)00046-C

[13] Pautsch, A. G., and Shedd, T. A., "Spray Impingement Cooling with Single- and Multiple-Nozzle Arrays. Part I: Heat Transfer Data Using FC-72," *International Journal of Heat and Mass Transfer*, Vol. 48, No. 15, July 2005, pp. 3167–3175. doi:10.1016/j.ijheatmasstransfer.2005.02.012

[14] Shedd, T. A., and Pautsch, A. G., "Spray Impingement Cooling with Single- and Multiple-Nozzle Arrays. Part II: Visualization and Empirical Models," *International Journal of Heat and Mass Transfer*, Vol. 48, No. 15, July 2005, pp. 3176–3184. doi:10.1016/j.ijheatmasstransfer.2005.02.013

[15] Lin, L., Harris, R., Lawson, J., and Ponnappan, R., "Spray Cooling with Methanol and Water Mixtures," 9th AIAA/ASME Joint Thermophysics and Heat Transfer Conference, AIAA Paper 2006-3410, San Francisco, June 2006.

[16] Puterbaugh, R. L., "The Effect of Dissolved Air on the Cooling Performance of a Partially Confined FC-72 Spray," M.S. Thesis, Dept. of Mechanical and Materials Engineering, Wright State Univ., Dayton, OH, 2008.

[17] Puterbaugh, R. L., Yerkes, K. L., and Thomas, S. K., "Partially Confined FC-72 Spray-Cooling Performance: Effect of Dissolved Air," *Journal of Thermophysics and Heat Transfer*, Vol. 23, No. 3, July–Sept. 2009, pp. 582–591. doi:10.2514/1.41654

[18] Baysinger, K. M., Yerkes, K. L., Michalak, T. E., Harris, R. J., and McQuillen, J., "Design of a Microgravity Spray Cooling Experiment," 42nd AIAA Aerospace Sciences Meeting and Exhibit, AIAA Paper 2004-966, Reno, NV, Jan. 2004.

[19] Yerkes, K. L., Michalak, T. E., Baysinger, K. M., Puterbaugh, R., Thomas, S. K., and McQuillen, J., "Variable-Gravity Effects on a Single-Phase Partially Confined Spray Cooling System," *Journal of Thermophysics and Heat Transfer*, Vol. 20, No. 3, July–Sept. 2006, pp. 361–370. doi:10.2514/1.18681

[20] Um, J., Sehmbey, M. S., and Chow, L. C., "Effects of Gravity on Spray Cooling," ASME International Mechanical Engineering Congress and Exhibition, American Society of Mechanical Engineers, Paper 96-WA/HT-26, Atlanta, Nov. 1996.

[21] Lin, L., and Ponnappan, R., "Heat Transfer Characteristics of Spray Cooling in a Closed Loop," *International Journal of Heat and Mass Transfer*, Vol. 46, No. 20, Sept. 2003, pp. 3737–3746. doi:10.1016/S0017-9310(03)00217-5

[22] Lin, L., Ponnappan, R., Yerkes, K., and Hager, B., "Large Area Spray Cooling," 42nd AIAA Aerospace Sciences Meeting and Exhibit, AIAA Paper 2004-1340, Reno, NV, Jan. 2004.

[23] Lin, L., and Ponnappan, R., "Two-Phase High Capacity Spray Cooling Loop—Nozzle Orientation Effects and Performance Results," 3rd International Energy Conversion Engineering Conference, AIAA Paper 2005-5733, San Francisco, 2005.

[24] Rybicki, J. R., and Mudawar, I., "Single-Phase and Two-Phase Cooling Characteristics of Upward-Facing and Downward-Facing Sprays," *International Journal of Heat and Mass Transfer*, Vol. 49, No. 1, Jan. 2006, pp. 5–16. doi:10.1016/j.ijheatmasstransfer.2005.07.040

[25] Mudawar, I., and Valentine, W. S., "Determination of the Local Quench Curve for Spray-Cooled Metallic Surfaces," *Journal of heat treating*, Vol. 7, No. 2, Sept. 1989, pp. 107–121. doi:10.1007/BF02833195

[26] Mudawar, I., and Estes, K. A., "Optimizing and Predicting CHF in Spray Cooling of a Square Surface," *Journal of Heat Transfer*, Vol. 118, No. 3, Aug. 1996, pp. 672–679. doi:10.1115/1.2822685

[27] Kato, M., Abe, Y., Mori, Y. H., and Nagashima, A., "Spray Cooling Characteristics Under Reduced Gravity," *Journal of Thermophysics and Heat Transfer*, Vol. 9, No. 2, Apr.—June 1995, pp. 378–381. doi:10.2514/3.675

[28] Sone, K., Yoshida, K., Oka, T., Abe, Y., Mori, Y., and Nagashima, A., "Spray Cooling Characteristics of Water and FC-72 Under Reduced and Elevated Gravity for Space Application," *31st Intersociety Energy Conversion Engineering Conference*, Vol. 2, Inst. of Electrical and Electronics Engineers, Piscataway, NJ, Aug. 1996, pp. 1500–1505. doi:10.1109/IECEC.1996.553950

[29] Yoshida, K., Abe, Y., Oka, T., Mori, Y. H., and Nagashima, A., "Spray Cooling Under Reduced Gravity Condition," *Journal of Heat Transfer*, Vol. 123, No. 2, Apr. 2001, pp. 309–318. doi:10.1115/1.1345887

[30] Roisman, I. V., Gambaryan-Roisman, T., Kyriopoulos, O., Stephan, P., and Tropea, C., "Breakup and Atomization of a Stretching Crown," *Physical Review E (Statistical Physics, Plasmas, Fluids, and Related Interdisciplinary Topics)*, Vol. 76, No. 2, Aug. 2007, pp. 026302-1—026302-9. doi:10.1103/PhysRevE.76.026302

[31] Gambaryan-Roisman, T., Kyriopoulos, O., Roisman, I., Stephan, P., and Tropea, C., "Gravity Effect on Spray Impact and Spray Cooling," *Microgravity Science and Technology*, Vol. 19, No. 3/4, 2007, pp. 151–154. doi:10.1007/BF02915782

[32] Rowden, B. L., Selvam, R. P., and Silk, E. A., "Spray Cooling Development Effort for Microgravity Environments," *Space Technology and Applications International Forum-STAIF 2006*, Vol. 813, AIP Conference Proceedings, American Inst. of Physics, Melville, NY, Feb. 2006, pp. 134–144. doi:10.1063/1.2169189

[33] Selvam, R. P., Lin, L., and Ponnappan, R., "Computational Modeling of Spray Cooling: Current Status and Future Challenges," *Space Technology and Applications International Forum-STAIF 2005*, Vol. 746, AIP Conference Proceedings, American Inst. of Physics, Melville, NY, Feb. 2005, pp. 55–63. doi:10.1063/1.1867118

[34] Selvam, R. P., and Ponnappan, R., "Numerical Modeling of Nucleation Boiling in Thin Film and Effect of Droplet Impact," *15th Annual*

Thermal and Fluids Analysis Workshop, NASA TFAWS04, Pasadena, CA, Aug. 2004.

[35] Selvam, R. P., Sarkar, M., and Ponnappan, R., "Modeling of Spray Cooling: Effect of Droplet Velocity and Liquid to Vapor Density Ratio on Heat Transfer," *16th Annual Thermal and Fluids Analysis Workshop*, NASA TFAWS05, Orlando, FL, Aug. 2005.

[36] Selvam, R. P., Sarkar, M., Sarkar, S., and Ponnappan, R., "Effect of Vapor Bubble Size on Heat Transfer in Spray Cooling," *Space Technology and Applications International Forum-STAIF 2006*, Vol. 813, AIP Conference Proceedings, American Inst. of Physics, Melville, NY, Feb. 2006, pp. 145–152. doi:10.1063/1.2169190

[37] Selvam, R. P., Sarkar, S., and Ponnappan, R., "Modeling of Spray Cooling: Convective Flow Effect on Vapor Bubble Dynamics and Heat Transfer," 9th AIAA/ASME Joint Thermophysics and Heat Transfer Conference, AIAA Paper 2006-3411, San Francisco, June 2006.

[38] Johnston, J. E., Selvam, R. P., and Silk, E. A., "Spray Cooling Modeling: Droplet Sub-Cooling Effect on Heat Transfer," *Space Technology and Applications International Forum-STAIF 2008*, Vol. 969, AIP Conference Proceedings, American Inst. of Physics, Melville, NY, Feb. 2008, pp. 104–111. doi:10.1063/1.2844942

[39] Cole, V., Mehra, D., Lowry, S., and Gray, D., "A Numerical Spray Impingement Model Coupled with a Free Surface Film Model," *16th Annual Thermal and Fluids Analysis Workshop*, NASA, TFAWS05, Orlando, FL, Aug. 2005.

[40] Baysinger, K. M., "Experimental Testing and Numerical Modeling of Spray Cooling Under Terrestrial Gravity Conditions," M.S. Thesis, Dept. of Mechanical and Materials Engineering, Wright State Univ., Dayton, OH, 2005.

[41] Elston, L. J., "The Effect of Variable Gravity on the Cooling Performance of a 16-Nozzle Spray Array," M.S. Thesis, Dept. of Mechanical and Materials Engineering, Wright State Univ., Dayton, OH, 2008.

[42] Elston, L. J., Yerkes, K. L., Thomas, S. K., and McQuillen, J., "The Effect of Variable Gravity on the Cooling Performance of a 16-Nozzle Spray Array," 47th AIAA Aerospace Sciences Meeting and Exhibit, AIAA Paper 2009-1025, Orlando, FL, Jan. 2009.

[43] Elston, L. J., Yerkes, K. L., Thomas, S. K., and McQuillen, J., "Qualitative Evaluation of a Liquid-Vapor Separator Concept in Micro-Gravity Conditions," *AIP Conference Proceedings CP1103: Space, Propulsion, and Energy Sciences International Forum: SPESIF-2009*, Vol. 1103, American Inst. of Physics, Huntsville, AL, Feb. 2009, pp. 3–13. doi:10.1063/1.3115546

[44] Elston, L. J., Yerkes, K. L., Thomas, S. K., and McQuillen, J., "Cooling Performance of a 16-Nozzle Array in Variable Gravity," *Journal of Thermophysics and Heat Transfer*, Vol. 23, No. 3, July–Sept. 2009, pp. 571–581. doi:10.2514/1.41653

[45] Shedd, T. A., "Next Generation Spray Cooling: High Heat Flux Management in Compact Spaces," *Heat Transfer Engineering*, Vol. 28, No. 2, Feb. 2007, pp. 87–92. doi:10.1080/01457630601023245

[46] Conrad, B. L., Springmann, J. C., McGill, L. A., and Shedd, T. A., "Effectiveness of Linear Spray Cooling in Microgravity," *Space, Propulsion, and Energy Sciences International Forum: SPESIF-2009*, Vol. 1103, AIP Conference Proceedings, American Inst. of Physics, Melville, NY, Feb. 2009, pp. 67–72. doi:10.1063/1.3115578

[47] Hunnel, C. A., Kuhlman, J. M., and Gray, D. D., "Spray Cooling in Terrestrial and Simulated Reduced Gravity," *Space Technology and Applications International Forum*, Vol. 813, AIP Conference Proceedings, American Inst. of Physics, Melville, NY, Feb. 2006, pp. 126–133. doi:10.1063/1.2169188

[48] Glaspell, S. L., "Effects of the Electric Kelvin Force on Spray Cooling Performance," M.S. Thesis, College of Engineering and Mineral Resources, Dept. of Mechanical and Aerospace Engineering, West Virginia Univ., Morgantown, WV, 2006.

[49] Kreitzer, P. J., "Experimental Testing of Convective Spray Cooling with the Aid of an Electrical Field Using the Coulomb Force," M.S. Thesis, College of Engineering and Mineral Resources, Dept. of Mechanical and Aerospace Engineering, West Virginia Univ., Morgantown, WV, 2006.

[50] Kreitzer, P. J., Glaspell, S. L., Kuhlman, J. M., Mehra, D., and Gray, D. D., "Electrical Force Effects on Spray Cooling," SAE Power Systems Conference, New Orleans, LA, Society of Automotive Engineers, Paper 2006-01-3064, Nov. 2006.

[51] Kuhlman, J. M., Kreitzer, P. J., Mehra, D., Gray, D. D., and Yerkes, K. L., "Influence of the Coulomb Force on Spray Cooling," *Space Technology and Applications International Forum-STAIF 2007*, Vol. 880, AIP Conference Proceedings, American Inst. of Physics, Melville, NY, Feb. 2007, pp. 100–109. doi:10.1063/1.2437446

[52] Kreitzer, P. J., Kuhlman, J. M., Mehra, D., Gray, D. D., and Yerkes, K. L., "Effects of Contact Charging on Spray Impingement Heat Transfer Performance and Spray Behavior," 39th AIAA Thermophysics Conference, AIAA Paper 2007-4269, AIAA, Miami, FL, June 2007.

[53] Kreitzer, P. J., and Kuhlman, J. M., "Visualization of Electro-hydrodynamic Effects and Time Scale Analysis for Impinging Spray Droplets of HFE-7000," *Space Technology and Applications International Forum-STAIF 2008*, Vol. 969, AIP Conference Proceedings, American Inst. of Physics, Melville, NY, Feb. 2008, pp. 86–93. doi:10.1063/1.2845053

[54] "Fluorinert Electronic Liquid FC-72 Product Information," 3M Company, St. Paul, MN, 2000.

[55] Geisler, K. J. L., "Buoyancy-Driven Two Phase Flow and Boiling Heat Transfer in Narrow Vertical Channels," Ph.D. Dissertation, Univ. of Minnesota, Minneapolis, MN, Feb. 2007.

[56] Michalak, T. E., "The Effect of Variable Gravity on the Cooling Performance of a Partially Confined FC-72 Spray," M.S. Thesis, Dept. of Mechanical and Materials Engineering, Wright State Univ., Dayton, OH, 2009.

[57] Yaniec, J. S., and Del Rosso, D., "JSC Reduced Gravity Program User's Guide: AOD 33899," NASA Aircraft Operation Div., Houston, TX, 2003.

[58] Yaniec, J. S., and Del Rosso, D., "Experiment Design Requirements and Guidelines NASA 931 KC135A: AOD 33897," NASA Aircraft Operation Div., Houston, TX, 2003.

[59] Yaniec, J. S., and Del Rosso, D., "Test Equipment Data Package Requirements and Guidelines NASA JSC RGO: AOD 33896," NASA Aircraft Operation Div., Houston, TX, 2003.

[60] Montgomery, D., and Runger, G., *Applied Statistics and Probability for Engineers*, 3rd ed., Wiley, New York, 2003, Chap. 8.

[61] Fox, R. W., and McDonald, A. T., *Introduction to Fluid Mechanics*, 5th ed., Wiley, New York, 1998, App. F.